THESIS

INVESTIGATING THE POTENTIAL OF MELTWATER AS A LOCAL SOURCE OF ICE NUCLEATING PARTICLES IN THE CENTRAL ARCTIC SUMMER

Submitted by

Camille Mavis

Department of Atmospheric Science

In partial fulfillment of the requirements

For the Degree of Master of Science

Colorado State University

Fort Collins, Colorado

Fall 2024

Master's Committee:

Advisor: Sonia Kreidenweis
Co-Advisor: Jessie Creamean

Jeffrey Pierce
Graham Peers

ABSTRACT

INVESTIGATING THE POTENTIAL OF MELTWATER AS A LOCAL SOURCE OF ICE NUCLEATING PARTICLES IN THE CENTRAL ARCTIC SUMMER

Due to climate change, the Arctic has crossed a threshold into positive feedbacks between sea-ice loss and increased absorption of solar radiation, causing warming up to four times the global average. Parameterizing the Arctic radiation budget to predict the new steady-state is paramount for guiding policies impacting future global socioeconomics and Arctic livelihoods. Arctic mixed-phase clouds (AMPCs) are a pillar in the feedback systems by modulating the surface energy budget, depending on the partitioning of cloudwater between ice and liquid phases that is sensitive to the concentration of ice nucleating particles (INPs) in the atmosphere. However, current observational gaps of central Arctic INP concentrations and sources may contribute to current challenges in resolving the controls on Arctic cloud ice content. The year-long expedition aboard the RV *Polarstern* from 2019 - 2020, entitled The Multidisciplinary drifting Observatory for the Study of Arctic Climate (MOSAiC), was a highly coordinated interdisciplinary effort that provided a unique opportunity to observe INPs in the central Arctic. The Arctic summer is a unique period characterized by pristine aerosol conditions, in which emissions from local sources have an increased influence, potentially impacting the ubiquitous low-lying AMPCs. Thus, the summer is an ideal season for exploration of the potential importance of INPs from local sources, such as melt ponds.
In this study, we used the Colorado State University (CSU) Ice Spectrometer and chemical treatments to determine the INP concentration and inferred composition in source samples of bulk sea water and meltwater from ponds and leads over the month of July. In addition, ambient aerosol filters were deployed both on the ship and on the ice, downwind of these meltwater features. We found that the concentration of INPs in meltwater was 10 times

higher than in the mixed layer of the ocean, a surprising result since previous studies did not see a difference in the two source samples. The INPs in meltwater were capable of freezing at temperatures (T) $\geq -10\,^{\circ}\mathrm{C}$ and were predominantly biological, based on our heating assay. Biological INPs capable of freezing at $\mathrm{T} \geq -10\,^{\circ}\mathrm{C}$ were present in 80 % of the on-ice aerosol samples. The alignment of slopes of the cumulative INP spectra between the meltwater and aerosol filter samples at $\mathrm{T} \geq -15\,^{\circ}\mathrm{C}$ suggested an influence from meltwater on the aerosol INPs at those temperatures. Similarities between aerosol INP sampled on the ice and on-board *Polarstern* suggested that the on-ice INP concentrations were likely influenced by a regional meltwater source signature, rather than being measurably impacted by a singular upwind pond. A relationship was observed between wind speed, supermicron particle counts, and on-ice aerosol INP populations active at warm ($-15\,^{\circ}\mathrm{C}$) and cold ($-25\,^{\circ}\mathrm{C}$) temperatures. A distinct on-ice aerosol sample containing no INPs active at $\mathrm{T} \geq -15\,^{\circ}\mathrm{C}$ was found to be influenced by southerly air over the ice-free ocean, emphasizing the potential impact meltwater may have as a unique source of warm temperature INPs in the central Arctic. These findings suggest that summertime central Arctic biological INP concentrations may increase if, as predicted, a spatio-temporal expansion of the melt season occurs in the near future. This increased INP concentration from local sources could impact central Arctic cloud microphysics, and thus their impact on the surface energy budget.

ACKNOWLEDGEMENTS

I would like to thank my advisor and co-advisor Sonia Kreidenweis and Jessie Creamean for their support of this project and for their thorough and thoughtful feedback during the writing process. I would also like to thank the other members of my committee, Jeffrey Pierce and Graham Peers, for their outside perspectives in thermodynamics and biology as input for my thesis. This work could not have been done if not for the technical expertise from members of the Kreidenweis research group including Kevin Barry, Tom Hill, Paul DeMott, and Carson Hume. Members of the MOSAiC science team Matthew Shupe and Emelia Chamberlain kindly engaged in discussions providing indispensable knowledge regarding the interdisciplinary aspects of this work. I would also like to thank other members of the MOSAiC atmospheric science team, Tuija Jokinen and Julia Schmale, for their involvement in collecting samples discussed in this work. I would like to thank my peers in the Atmospheric Science program, as well as my friends and family, for their support throughout this project, both academically and personally.

TABLE OF CONTENTS

LIST OF TABLES

LIST OF FIGURES

Chapter 1

Introduction

1.1 Climate change and INPs in the Arctic

1.1.1 Arctic amplification

The Arctic has entered a phase of rapid transformation[1] due to climate change, with the region warming up to four times faster than the global average.[2] This accelerated warming, driven by positive feedback loops between sea-ice and glacier loss and increased solar absorption,[3,4,5] underscores the importance of resolving its radiation budget for realistic projections of regional and global climate. Currently, the largest source of uncertainty in projections of global temperature change stems from aerosol-cloud interactions,[6] processes which are particularly complex in the Arctic. Arctic mixed-phase clouds (AMPCs), which contain both liquid and ice phases, are especially influential on the surface radiation budget.[7,8,9,10] The partitioning of liquid and ice in these clouds modulates the radiation reaching the surface,[7,8,9,10,11] impacts cloud lifetime,[12,13,14] and is highly sensitive to the atmospheric concentration of ice nucleating particles (INPs),[12,13,14,15,16] which initiate freezing in supercooled droplets. Filling gaps in observations of INPs in the central Arctic[17] is needed for achieving greater certainty in determining cloud ice content for modeling the amount of radiation that reaches the surface,[18] values which can ultimately impact the extent of sea ice melt, melt onset, and seasonal sea ice minima.[19,20,21,22]

1.1.2 Possible climate-driven changes to terrestrial and marine INPs in the high-latitudes

As the Arctic undergoes rapid terrestrial and oceanic changes as a result of global warming, local sources of cloud-active aerosols, including INPs, are also evolving. Arctic and sub-Arctic regions are experiencing intensified wildfire seasons,[23,24] thawing permafrost, and

glacial retreat, each contributing new potential sources of INPs. Emissions from biomass burning, including wildfire smoke, have been linked to INP production[25,26,27] and even influenced cloud formation.[28] Additionally, thawing permafrost and glacial retreat are exposing previously trapped biological and mineral particles that may also serve as INPs.[29,30,31] In terms of the Arctic Ocean, a major consequence of Arctic amplification is the dramatic, seasonal decline in sea ice.[32] Thicker, brighter[33] multi-year ice is rapidly[34] being replaced by thinner, first year ice,[35,36] driving changes in the surface energy balance, dynamically-driven[37,38] local biological processes,[39,40,41] and the interface between the ocean and atmosphere,[42,43] which may affect sea spray aerosol[44,45] and biogenic emissions.[46,47,48,49]

1.1.3 Seasonally driven INP observations

The influences of terrestrial sources on high-Arctic INPs have a strong seasonal dependence, driven by large-scale atmospheric patterns. Influences from lower latitudes on Arctic aerosol is due to wintertime "Arctic Haze,"[50,51] which typically contains low concentrations of INPs that are not as effective at freezing at warmer temperatures.[52,53] In the summer, warmer surface temperatures lead to instability and convection within the air masses en route to the central Arctic, providing more efficient removal processes for transported particles (i.e., from precipitation during transport).[50,54,55] Conditions for horizontal advection of particles from lower-latitude sources are less favorable in the summer due to the shrinking of the polar dome, lending prominence to natural aerosols from regional sources.[50] This pattern was observed by Creamean et al., (2022)[56] in which the general sources and composition were found to be long-range terrestrial and inorganic in the winter and local marine and biogenic during the summer. Local marine sources of INPs have been attributed to the open ocean[57,58,59] or leads within the pack-ice,[60] however, specific sources of high Arctic local INPs are still unknown. Other studies have reported enhanced levels of warm-temperature (active at $T \geq -15$ °C) INPs during summer months at terrestrial[61,62,63] and near-coast, ship-based[59] sites in the Arctic that could be attributed to biogenic or fungal species from

coastal waters or land. However, the observed increase in biological INPs and the correlation with melt pond fraction reported in Creamean et al. (2022) and Barry et al. (2024)[64] suggest that melt-related processes within the pack ice, such as the formation of melt ponds and the resulting meltwater layer on the sea ice and open ocean, may be a potential source of INPs.

1.1.4 The melt water interface

Melt water is a low-salinity, liquid interface between the sea-ice and atmosphere comprised of melted snow and sea ice that is unique to the Arctic summer. This liquid interface between the sea ice and atmosphere could act as a potential conduit for bioaerosols associated with organisms habitating in the sea ice,[65] snow,[66] and unique meltwater environments[42,67] whose cold-adapted, proteinaceous[68,69] or organic material[70] may act as effective INPs. Emission mechanisms from shallow melt ponds have not been identified in part due to a lack of observations. It is so far assumed that generation of aerosol from a liquid surface involves bubbles, in which surface-active,[71] biogenic,[72] and scavenged[73] material from the water is ejected into the air upon bubble bursting. Wind-independent bubble generation has been suggested for low-fetch surfaces in low-wind conditions[74] including melting snow-flakes on the surface[75] or the release of trapped air bubbles within the ice as it melts.[76,77] Additionally, ripples generated by wind or movement of the sea ice on the melt pond surface may be capable of releasing aerosol via bubble-bursting in which a high supersaturation of dissolved gasses within the meltwater could increase the efficiency of aerosolization.[78] The ephemeral quality of this interface may diminish as the duration of melt season increases[79] and trends northward,[80] causing the area of open water and leads covered by a layer of meltwater[42] to expand. As this expands, it could change the capacity for INPs from meltwater to become airborne. In addition, higher fetch over meltwater surfaces will increase the relevance of wind-driven processes of aerosol generation. Enhanced storminess in the summer[81] may also induce more vertical mixing[37] of the stratified melt and upper ocean layers, creating a combined

INP population within the mixed layer of the Arctic Ocean, influenced by meltwater. The frequent occurrence of AMPCs with low-altitude bases and significant ice content,[56,82,83] and atmospheric patterns favoring local sources of aerosol during the summer, emphasizes the need to characterize the potential emissions of INPs from this source during this period.

1.2 The MOSAiC field campaign

The year-long Multidisciplinary drifting Observatory for the Study of Arctic Climate 2019-2020 expedition (MOSAiC) aboard the icebreaking German research vessel (RV) *Polarstern*[84] intended to address gaps in knowledge related to the representation of Arctic coupled systems in models in the context of a rapidly changing climate. The *Polarstern* embarked from the Norwegian coast in September 2019 to north of the Laptev Sea where it moored into an ice floe and traveled passively from October 2019 - August 2020 via the transpolar drift, which transports surface waters and sea ice from the Laptev Sea and the East Siberian Sea towards the Fram Strait. Upon break-up of the original floe, *Polarstern* transited back north into the pack ice August - September 2020 to close out the annual cycle within the ice.[85] The journey was separated into five legs from October 2019 to September 2020 (**Figure 2.1**) with two periods of transit in between. The interdisciplinary scientific aims of MOSAiC required a sampling program involving teams focused on the atmosphere, physical oceanography, sea ice and snow, ecology, and biogeochemical measurements. Hundreds of researchers from across 20 nations were involved in the effort,[86] which resulted in a suite of co-located observational platforms and an abundance of data that primed the way for cross-disciplinary investigations, such as this one. Details on the expedition and Central Observatory (CO) surrounding *Polarstern* are described by Shupe et al. (2022),[87] Nicolaus et al. (2022),[88] Rabe et al. (2022),[89] and Fong et al. (2024).[90] In this study, we investigated the potential of melt ponds as local sources of INPs in the high Arctic, focused on samples collected in July 2020 of the MOSAiC campaign.

1.3 Science aims and questions

The questions addressed in this study were embedded within the broader questions posed by the atmospheric science team of MOSAiC.[87] To summarize, how are sea ice processes coupled to atmospheric, oceanic, and ecosystem processes? And what are the processes that regulate Arctic cloud dynamics and their interactions with aerosols, boundary layer structure, and atmospheric fluxes? We aim to better understand how sea ice melt is coupled with the atmosphere via INPs and the implications for cloud properties. Collected samples and subsequent analyses contribute to a dataset of central Arctic INP observations to achieve realistic constraints for models simulating Arctic cloud phase,[18,87] such as a potential relationship between ponded sea ice surface area and source flux of INPs. Novel parameterizations[91] of INP concentration have improved simulated cloud-ice but fail to capture rare, warm temperature INPs, especially in a unique environment like in the high Arctic. We hope to narrow the uncertainties associated with Arctic aerosol-cloud interactions by addressing the following questions:

- Meltwater: What are the INP concentrations and compositions in central Arctic meltwater samples from July 2020 and how do those concentrations compare with other sources such as sea water, snow, and ice cores? What can be said about the relative importance of meltwater as a local source of INPs in the central Arctic?

- Air: What are the concentrations and compositions of airborne INPs collected on filters deployed near the surface, downwind of the meltwater sampling locations, and how do the concentrations compare with INPs collected using higher volume filter samplers located on the *Polarstern* during the same period?

- Coupling: How do the INP temperature spectra in meltwater sources and near-surface aerosol filters compare to each other, and what can be determined from local meteorology regarding conditions that are favorable for a local influence of meltwater sources on airborne INPs?

Chapter 2

Methods

2.1 MOSAiC expedition details and sampling platforms

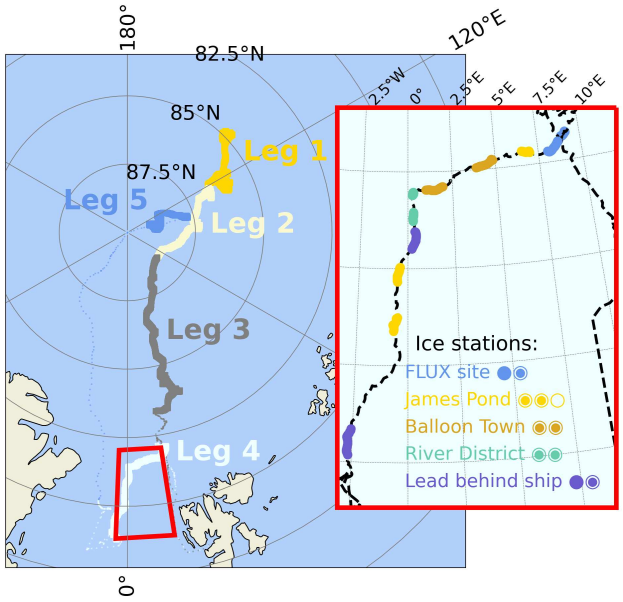

Figure 2.1: (Left) *Polarstern* drift track during the MOSAiC 2019-2020 expedition. Bold points mark passive drift: October 4-December 13 (Leg 1); December 13-February 24 (Leg 2); February 24-May 16 (Leg 3); June 19-July 31 (Leg 4); and August 21-September 20 (Leg 5). (Right) Leg 4 zoom-in marking the Lagrangian tracks of the ice station locations within the Central Observatory as the floe drifted. Solid, open, and fish-eye circles signify ice stations where aerosol filter, meltwater, or both samples were collected, respectively.

Here, we report on discrete samples of aerosols (on-board aerosol filters) and bulk seawater (BSW) collected on-board *Polarstern*, and sea ice, snow, and meltwater samples collected in the CO, as described in detail by Barry et al. (2024) and Creamean et al. (2022), for offline INP analyses. During Leg 4 (29 June - 28 July 2020), we additionally collected filter samples of aerosol using a portable aerosol sampling package deployed directly on the ice in the CO, near open meltwater sources (on-ice aerosol filters). As shown in **Figure 2.1**, the on-ice sampling locations within the CO were referred to as Flux Site, James Pond,

Balloon Town, River District, and Lead, and all were within 1 km from *Polarstern* (**Figure A.1**). The non-aerosol samples were collected to assess INP concentrations in potential local sources ("source" sample). Supporting real-time aerosol size distributions and number concentrations from *Polarstern*'s P-deck (uppermost deck above the bridge) and meteorological variables from Met City in the CO were used as context for the INP data. Details on discrete sample collections and real-time datasets are described in detail in the following sections.

2.2 Discrete sample collection for INP analysis

2.2.1 Aerosol filters collected on the ice

A portable aerosol package (called "C3PO") was deployed during Leg 4 for on-ice collection of aerosol samples downwind of open meltwater sources (**Figure 2.1**). The package included a miniaturized custom-built time-resolved aerosol particle sampler (TRAPS) as described by Creamean et al. (2018),[92] a 12V Brailsford vacuum pump (TD¬4X2N), and 12V automotive battery to power the pump and TRAPS for up to several days. Aerosols were collected on pre-cleaned filters (Pallflex® Emfab™ 47 mm borosilicate glass microfiber) loaded in the TRAPS. These filters were pre-cleaned by soaking in nitric acid (Fisher Chemical, Certified ACS Plus) for 5 days, triple-rinsed with deionized water (DI), and then laid to dry in a laminar flow cabinet. Each filter from the TRAPS collected air for 26-30 hours, collecting a range of volumes (341-1077 sL). Due to the pristine air, time-resolved samples were combined to obtain sufficient aerosol loading for the INP measurements. Details on each TRAPS sample are provided in **Table A.1**. A field-blank filter was collected during a deployment (July 23) in which the vacuum pump malfunctioned, and total filtered air was 0 sL. After deployments of C3PO, sampled filters were preserved and transported frozen ($\leq -20^{\circ}$C) in sterile petri dishes similar to filters collected on *Polarstern* (Barry et al., 2024) prior to INP analysis 36-37 months after the MOSAiC expedition at CSU.

2.2.2 Aerosol filters collected on *Polarstern*

Since details on these samples are described by Barry et al. (2024), they are only briefly reiterated here. The total aerosol filter sampler was mounted on board *Polarstern*'s P-deck on top of the U.S. Department of Energy Atmospheric Radiation Measurement (DOE ARM) AMF2 facility, at a height of 15 m above sea level. Polycarbonate filters (0.2 μm and 10 μm Whatman Nuclepore track-etched hydrophilic membranes for sample and backing filters, respectively) were collected for the duration of the entire campaign over 72-hour integration times, averaging total filtered air volumes of 88,800 sL per sample. As such, they represent a longer-term data record representative of the study region. The polycarbonate filters were prepared as described by Barry et al. (2024). Sampled filters were stored and transported frozen (≤ -20 °C) in sterile petri dishes prior to INP analysis at CSU.

2.2.3 Source samples

Details on the general collection of seawater, meltwater, and sea ice and snow are outlined in Rabe et al. (2022), Shupe et al. (2022), Fong et al (2024), and Nicolaus et al. (2022), and are briefly summarized below. For the INP samples specifically, both seawater and meltwater samples were collected manually in triple-rinsed 50 mL centrifuge tubes. The seawater samples were collected approximately daily from a single tap of *Polarstern*'s flowthrough seawater system, which intakes water at 11 m depth. Meltwater samples were collected during Leg 4 C3PO deployments upwind of the aerosol sampler (**Table A.1**), in which water was sampled by hand from the edge of these open water features. Snow was sampled approximately weekly combined with snowpit measurements. The snow samples were collected by pressing a 50 mL centrifuge tube into the side of the pit at a variety of depths (surface, middle, and near the snow-ice interface) and filled to the top. Both first- and second-year ice cores were collected approximately weekly using a 9-cm diameter KOVACS Mark II coring system and sectioned in-field into sterile Whirl-Pak^{TM} bags. Adjacent core segments from the same depths were combined by melting at room temperature, then diluted with filtered

seawater (FSW) (0.22 μm Millipore Sterivex), and parsed into triple-rinsed 50 mL centrifuge tubes under red-light only, temperature-controlled conditions aboard *Polarstern*. The daily seawater and weekly snowpit and ice core sampling occurred throughout the expedition, however, the subset of samples discussed herein coincided with the on-ice observation periods of June and July. All source samples were stored and transported frozen (≤ -20 °C) prior to INP analysis at CSU.

2.3 Ice nucleation measurements

For the aerosol samples, particles were removed from the on-board and on-ice filters by adding a volume (8 mL and 6 mL, respectively) of 0.1 μm filtered DI water in a pre-rinsed 50 mL centrifuge tube into which the sample filters were carefully transferred with clean tweezers. The particles were then incorporated into suspension via rotation for 20 minutes in a Roto-Torque rotator (Cole Parmer).

Solutions for meltwater, ice core, and snow were prepared by thawing collected samples at room temperature without further processing. Due to the addition of FSW to the ice core samples, a representative flowthrough sample (same sample date as ice core) was filtered with a 0.22 μm Millipore Sterivex pressure filter and tested for INPs. The FSW INPs were then subtracted from the ice core sample INP concentrations according to the meltwater factor (**Table A.4**).

All prepared sample solutions were diluted (11-fold: 400 μL sample and 4000 μL 0.1 μm filtered DI water) and pipetted out in 50 μL aliquots into PCR trays (Optimum Ultra) using 32 wells for each dilution. For each sample, 32 additional wells were designated for a negative control of 0.1 μm filtered DI. The PCR trays were then fitted into the notched aluminum blocks of the CSU Ice Spectrometer (IS) and cooled at 0.33 °C/min while a camera recorded the number of frozen wells every 18 seconds. The IS configuration and procedure are further described in Creamean (2024)[93] and the references therein. The number of frozen wells was first converted to concentration of INPs per mL of suspension, then upon accounting for total

volume of air filtered, converted to INPs per standard liters (sL) air based on Vali (1971).[94] Equation 2.1 was used to calculate a conversion factor (0.9868) between air volume measured by the TRAPS (V) to air volume at standard temperature and pressure (V_{STP}, sL). Values for T and P are median temperature and pressure for July 2020 of MOSAiC reported by Rinke, et al (2021)[95] and T_{STP} and P_{STP} are standard temperature and pressure (273.15 K, 1013.25 hPa). 95 % confidence intervals were calculated based on Agresti and Coulli (1998).[96] The INP concentrations presented herein are averages and include the values for the 95 % confidence interval in parentheses. To correct for the field blank, concentrations of INPs/mL of solution retrieved from the field blanks were subtracted from the samples across the temperature spectrum at 0.5 °C resolution before conversion to INPs/sL air.

$$\frac{V_{STP}}{V} = \frac{T_{STP}}{P_{STP}} \frac{P}{T} \tag{2.1}$$

Treatments were applied to aliquots of the 5 meltwater samples and 4 on-ice filter samples to infer INP composition, as reported in previous studies.[97,98,99] Specifically, thermal (95 °C) and chemical (hydrogen peroxide, H_2O_2) treatments were applied as was done to the filters collected on *Polarstern*'s P-deck (Barry et al., 2024). Briefly, aliquots of the sample solutions were heated for 20 min at 95 °C to destroy heat labile (proteinaceous) material. The addition of 1 mL 10 % H_2O_2, followed by 20 min of heating at 95 °C and exposure to UV-B light to another aliquot of the sample solution removes all organic material by the digestion of remaining heat stable material. The reduction of INPs between the neat (heated) and heated (digested) samples are presumed as proteinaceous (organic) sample constituents. The INP remaining after the peroxide treatment are presumed to be the inorganic (mineral) constituent. Treatments were also applied to a blank Emfab filter to provide corrections for the treatment data.

2.4 Salinity measurements on water samples

Salinity of the meltwater and BSW samples was measured to correct their cumulative INP spectra for salt freezing point depression. First, the conductivity of the samples was measured using an EXTECH ExStikII EC400 TDS/Conductivity/Salinity Pen (0 to 199.9 μS/cm, 200 to 1999 μS/cm, 2.00 to 19.99 μS/cm $\pm 2\,\%$ full scale accuracy) at 25 °C. Next, salinity (g/kg) was derived from conductivity using an online calculator employing the 1983 UNESCO algorithm.[100] The samples were diluted 5-fold with DI water. The freezing point depression factor was calculated using the Van't Hoff relationship (Eq. 2.2). The molality of each sample (m) was calculated from their salinities with the assumption that the major ionic composition is NaCl (molecular weight = 58.44 g/mol). The Van't Hoff factor, $i = 2$, and the freezing proportionality constant of water, $K_f = 1.86$.

$$\Delta T = iK_f m \tag{2.2}$$

The cumulative INP spectra for the water samples were corrected by adding the freezing point depression factor, ΔT, to the observed freezing temperatures.

2.5 Supporting Datasets

2.5.1 Meteorological data

The air temperature and winds presented here were measured 2 m above the sea ice with a Vaisala PTU300 sensor and Metek uSonic-3 Cage MP sonic anemometer (respectively) fixed to a 10 m meteorological tower located at Met City within the Central Observatory.[101] Both temperature and wind data sets had a time resolution of 1 minute, and were averaged over the air-filter sampling periods to the nearest hour (**Figure A.2**). The wind speed was expressed using a Matplotlib boxplot function (medians; Q1 - Q3; and Q1-1.5(IQR), Q3+1.5(IQR)).[102] The wind direction was expressed through a cyclic color bar representing the median wind directions utilizing NumPy.[103]

2.5.2 Aerosol number concentrations and size distributions

Particle number size distributions (diameters 1.06 to 16.1 μm) were measured continuously by an Aerodynamic Particle Sizer spectrometer (APS, model 3321, TSI Incorporated, Minnesota, USA) located behind an inlet with upper cutoff size of 40 μm and flow of 10 L/min, located in the Swiss container (near the DOE container) on the D-deck of *Polarstern*. Particle number concentrations were measured with the aforementioned APS and by a condensation particle counter (CPC) model 3025 from TSI Inc., with minimum detectable particle diameter = 3 nm and time a resolution of 10 s, located behind an inlet with a flow of 0.3 L/min (odd hours: interstitial, even hours: total aerosol) in the Swiss container on the D-deck of *Polarstern*. Aerosol concentration data from the APS and CPC were pollution-flagged using a five-step pollution detection algorithm (PDA) described in Beck et al. (2022).[104] The APS data were averaged to 1-minute time intervals and corrections were applied according to Bergner et al. (2023).[105] The CPC total number concentration data were corrected to address step changes in concentration associated with valve switches between the interstitial and total air inlet.[106] For this study, the quality-controlled and pollution-filtered aerosol data were averaged over each sample day from 00:00:00 to 23:59:00 UTC.

2.5.3 Air mass trajectory and sea ice concentration data analysis

The relative air mass residence times (seconds) over different surface types were calculated using FLEXPART simulations[107] every 3 hours for a 100 m air tracer species aged 0.25, 1, 7, 10, and 30 days and the Multisensor Analyzed Sea Ice Extent (MASIE) product and ice concentration from the Advanced Microwave Scanning Radiometer 2 (AMSR2), or MASIE-AMSR2 (MASAM2) for daily 4 km Sea Ice Concentration (Version 2).[108] First, the MASAM2 4 x 4 km cartesian grid data were re-gridded to match the FLEXPART (0.25 x 0.5) geospatial data using Python's xESMF: Universal Regridder for Geospatial Data package.[109] Then, for every grid point where (s) was greater than 0, the surface type was determined by the

following sea-ice concentration (%) thresholds as defined by the Norwegian Polar Institute (values 1 to 39 not used by MASAM2): open ocean = 0, marginal ice zone = 40-85, pack-ice = 85-100, and land = 120. The surface types were determined for every grid point over a domain of (90N, 60S, 60W, -60E) for each 3-hour FLEXPART simulation during each on-ice filter sample period. For each simulation, the number of grid points per surface classification was counted, then averaged over the whole day (sample period), and normalized by daily-averaged total counts to yield relative surface area fractions traversed by the air mass. Superimposed 3-hour FLEXPART trajectories over sea ice concentrations for each sample day are shown in **Figure A.3**.

Chapter 3

Results and Discussion

3.1 Context from prior studies

Before diving into the specific meteorological, aerosol, and melt variables for on-ice sampling days, we present an overview of these variables during the MOSAiC summer (Leg 4) as reported from previous work.

3.1.1 Meteorology

Overall, the MOSAiC summer was anomalously warm and wet, driving an extended melt season.[87,95] The 2020 Central Arctic summer experienced temperatures 5 °C above the 1981-2010 mean temperature.[110] Additionally, melt conditions lasted over a month longer than 1979-2019 median.[95] The monthly median total column water vapor concentrations in July and August 2020 had the highest warm anomalies compared to the 1970-2019 medians.[95] This high moisture content affected both atmospheric vertical structure and surface melt conditions. The high occurrence of clouds in the summer has been linked to the erosion of typically strong surface inversions,[111] and it was often observed during the MOSAiC summer that a stable layer "capped" a well-mixed boundary layer.[112] The temperature, wind speed, and precipitation averages for the month of July 2020 are as follows: the median (min, max) 2 m temperature and 10 m wind speeds were 1 (0, 2.6) °C and 4 (1.5, 9.4) m/s, respectively.[95] **Figure 3.1** shows the daily-average precipitation rate as measured by the weather detector on the Met City tower at the Central Observatory in which the average daily precipitation rate for the month of July was 0.027 mm/hr. July 2 was anomalously high in daily-average precipitation rate (0.22 mm/hr, $\sigma = 0.46$ mm/hr), which was 4.34 standard deviations higher than the monthly mean and was notably liquid precipitation.[113] Rain in the central Arctic is rare, however it is becoming more common[114] and rain-dominated precipitation is projected

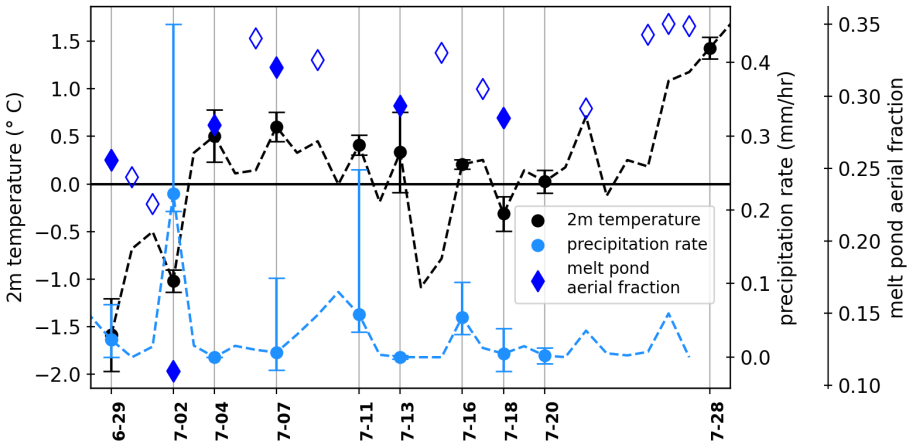

Figure 3.1: Time series (on-ice sample days shown as filled symbols) of daily-averaged values of 2 m temperature (black dash (black circles)), rain-rate as measured by the Met-City PWD (light blue dash (light blue circles)) and melt pond aerial fraction (blue diamond hollow (filled)). Melt pond aerial fractions were calculated from the University of Bremen109 within a 1 x 1 degree domain around *Polarstern*.

to increase,[115,116,117] which has implications for the scavenging of both local and transported aerosol.

3.1.2 Surface melt

Surface temperature, snowfall, and rainfall drove variability in early season melt pond (MP) aerial fraction (Webster, 2022).[113] The onset of surface melt was May 25[118] and by May 28, widespread ponded surfaces were observed via satellite,[113,119] driven by southerly air and thick clouds.[118] Later stages of MP formation and drainage during the summer were unevenly distributed in time[113] and may be a function of surface topography and snow distribution on different ice types.[120,121] In addition to forming ponds on the sea ice, meltwater can collect on every water surface including leads and cracks in the pack ice, open spaces within ice ridges, and underneath the ice.[42] During the Leg 4 Central Observatory (June 29-July 26) on the main floe, the *Polarstern* predominantly transected second year ice (SYI), with first year ice (FYI) mostly present during the last third. Some notable events that influenced the timeline of MP areal fraction (**Figure 3.1**), as summarized from Webster et al. (2022) include:

- June 29: Below freezing temperatures refroze the surface of some MPs creating an "ice lid" and decreased areal fraction by 1 %
- July 2: Heavy precipitation increased MP areal fraction and depth
- July 11-13: Drainage from a large pond decreased overall areal pond fraction from 21 to 15 %
- July 16: Maximum weekly averaged rate of surface ice melt[122]
- July 21: MP depth maximum (FYI: 22 ± 13 cm; SYI: 29 ± 14 cm)
- July 26: MP area maximum (21 %, depth 19 ± 11 cm) with thin 3-5 mm ice layer

The above values of melt pond area fraction were retrieved from in-situ transect data, representing melt ponds from a smaller domain than in **Figure 3.1** in which the melt pond area fraction was calculated from Sentinel-3 satellite retrievals[123] within a 1x1 degree grid surrounding the *Polarstern*.[56]

3.1.3 Aerosols

There was a seasonal shift in the aerosol particle number size distribution during the MOSAiC campaign. Boyer et al. (2023) reported that a single mode centered at 100 nm from October 2019 - April 2020 shifted to a bimodal distribution beginning in May 2020 with a secondary mode centered in the Aitken regime.[124] The shift in particle size distribution with the enhancement of solar radiation suggests new particle formation (NPF) due to emissions of gaseous precursors by local biological activity. Uncertainties remain regarding NPF in the Arctic[17] and nucleation-mode particles are not expected to affect INPs.[125] However, other processes associated with biological activity, such as bubble formation due to respiration or secretion of exopolymeric substances (EPS), have been linked to INPs in the Arctic.[126,127] The monthly average concentrations of supermicron aerosols were lowest in summer (June - August). However, monthly-averaged aerosol INPs active at T = −20 °C reached an annual

maximum in June and July with the largest fractions from the $1.2 - 3.0\ \mu$m size range.[56] Studies conducted at various locations show coarse-mode aerosol ($> 2.5\ \mu$m) to be associated with high ice nucleating activity.[57,92,128] In terms of marine environments, INPs larger than 0.2 μm[129] may represent intact or fragmented cells of diatoms.[130,131] Measurements of fluorescent aerosols suggest seasonal variability between sources. Total excited aerosols were highest during the Arctic haze season (November 2019 - April 2020) and lowest in the summer (June - September 2020).[132] However, the fractions of fluorescent (FA) and hyperfluorescent (HFA) particles were highest in the summer,[132] peaking in June. HFA have been reported as strongly influenced by biological sources.[133,134] The composition of June HFA particles were mostly types A and AB[132] which can be attributed to bacterial, fungal, and algal influences.[135]

3.2 Aerosol INPs downwind of meltwater features

INP concentrations measured from the aerosol filters collected downwind of surface meltwater features are shown in **Figure 3.2** as a time series of the cumulative INP concentrations active at select temperatures. The full temperature spectrum of cumulative INP concentration within 95 % confidence for each sample is shown in **Figure A.4**. From herein, the lowest common temperature at which all samples commonly had a signal (-29.0 °C) will serve as a proxy for total INP concentration.

Total INP concentrations across the on-ice aerosol filters spanned five orders of magnitude: from 3.5×10^{-3} (1.6×10^{-3}, 5.7×10^{-3}) INP/sL on July 2 to 1.98×10^{2} (53.3, 2.44×10^{2}) INP/sL on July 4 (July 28 was notably high: 1.68×10^{2} (75.9, 2.63×10^{2} INP/sL). This span in magnitude can be attributed to both local and regional meteorological conditions. First, it is evident that the filter from July 2 was affected by precipitation and low melt pond fraction as inferred from Figures A.5 and 3.1. Total INP concentration on this date was three orders of magnitude lower than the typical concentration observed in the other samples, and no INPs with freezing temperatures warmer than -15.0°C were detected (**Figure A.4**). The low melt

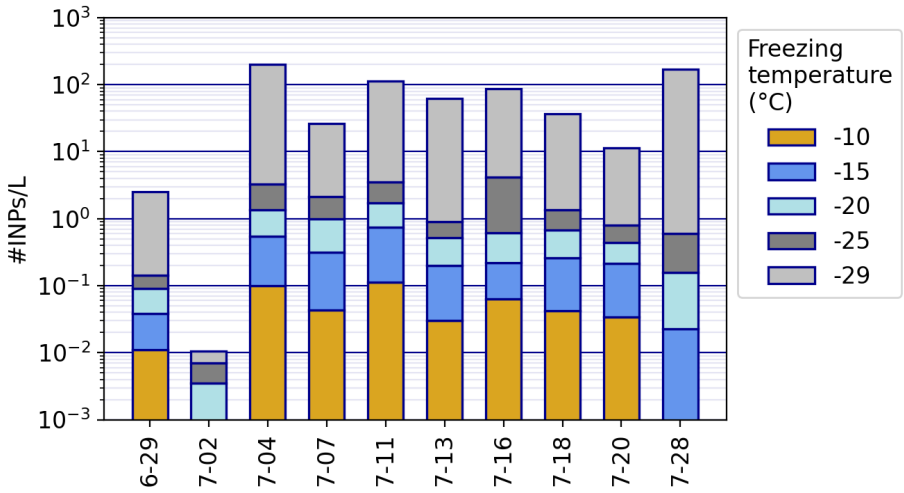

Figure 3.2: Concentration of INPs/sL collected on on-ice aerosol filters. Cumulative concentrations measured at different temperatures are shown by the corresponding color bars.

pond fraction was likely a consequence of the daily-averaged, below-freezing 2 m temperatures that formed ice-lids days prior to July 2 (discussed below), potentially cutting off the meltwater source of INPs. Additionally, supermicron aerosols are more efficiently scavenged than submicron,[136] and bioaerosols are often in the supermicron regime,[125,137,138,139,140] so it is likely the lack of INPs active at T $\geq -15\,^{\circ}$C was due to scavenging by precipitation. The July 28 sample had the second-highest total INPs, however did not have any INPs active at T $\geq -15\,^{\circ}$C. This can be attributed to a different source region, discussed in **Section 3.5.2**.

The filter with the lowest total INP concentration for rain-free days occurred on June 29 at 2.37 (0.65, 6.71) INP/sL. On that day, the daily-averaged 2 m air temperature was $-1.5\,^{\circ}$C and did not reach above freezing until July 3 (**Figure 3.1**). C3PO was sampling air during this period from June 29 12:00 to June 30 16:00 UTC. The freeze-up created ice-lids on the early-season melt ponds and an associated decrease in melt pond aerial fraction (within a 1x1 degree grid around *Polarstern*) of 1.2, 3.1, and 14.6 % from June 29 to June 30, July 1, and July 2, respectively. This freeze-up may have decreased any potential upwind meltwater source influences on the June 29 on-ice aerosol INP. Despite the lower total INPs on this date, the fractions of INPs active at T $\geq -25\,^{\circ}$C within the total are relatively similar to the other rain-free samples. The next filter that was collected during above-freezing conditions

was on July 4, when the melt pond aerial fraction had increased by 2.4 % from June 29. This increase in surface meltwater may be attributed to the above freezing temperatures and precipitation on July 2.

Figure 3.2 highlights the apparent commonalities in the INP from rain-free on-ice aerosol filters collected from July 4 to July 20. The INP concentration distributions across temperatures were similar, notably the INPs active at T$\geq -10\,^{\circ}$C, with concentrations consistently between 0.03 - 0.1 INP/sL. The highest onset temperature across all on-ice aerosol INPs was $-8.6\,^{\circ}$C ($-8.7\,^{\circ}$C) for July 11 and July 16 (July 4). Note that the onset temperature is a qualitative measure due to detection limits; warmer temperature INPs could be present in the atmosphere. As will be discussed below, heat treatments, as described in the methods, indicated that the warm-temperature INPs in those samples were associated with proteinaceous (biological) material. The cumulative spectra in **Figure A.4** suggest the presence of a mode of INPs that activated near T= $-10\,^{\circ}$C, and another population that dominated at temperatures below $-25\,^{\circ}$C. The mode and overall spectral shapes above T= $-20\,^{\circ}$C are typically associated with INPs of biological composition.[57,141] It is widely assumed that only proteinaceous (biological) material can nucleate at such warm temperatures within the class of natural aerosols, due to the properties favorable to ice crystal formation within protein structures.[130,139,142,143,144,145,146,147]

3.3 Characterizing INPs in meltwater sources

The analysis of the meltwater samples revealed the potential for meltwater as a local source of INPs in the Arctic. The ice nucleation capacity is noteworthy in both dimensions of measurement: the warmest detected freezing temperature and INP number concentration. Regarding the first, all samples contained INPs capable of freezing at T $\geq -15\,^{\circ}$C. With the exception of July 4 ($-12.5\,^{\circ}$C freezing onset), all samples reached nucleation temperatures greater than $-10\,^{\circ}$C and up to $-6.5\,^{\circ}$C (July 28), suggesting the presence of biological INPs (see **Section 3.4**). The second notable point is the overall number concentration of

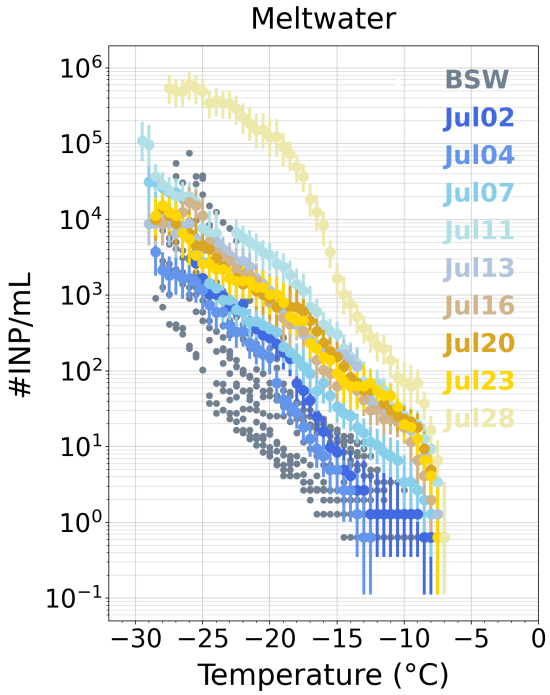

Figure 3.3: Cumulative INP concentration as a function of temperature for July meltwater (colored) and annual bulk sea water (gray) sampled during MOSAiC 2019-2020. 95 % confidence intervals are shown for the meltwater samples.

INPs/mL in the meltwater compared to the BSW samples from the same time period. These findings contrast with previous studies that found no significant difference between water samples from melt ponds and the ice free ocean.[59,148] Meltwater samples between July 11 - July 23 were consistently tenfold greater in INP concentrations than the BSW samples from −10 to −25 °C, and July 28 was nearly one hundred fold greater between −10 to −25 °C, and about a thousand fold greater from−10 to −25 °C. The July 28 meltwater sample is singular in that it was taken from a lead, located behind the *Polarstern*. The sample salinity was 1.54 g/kg indicating this sample was taken from a meltwater layer at the surface of the lead. The meltwater layers that form over leads, as opposed to on top of sea ice, may harbor distinct biological communities influenced by the interface between the meltwater and sea water below, driving the INP variability in this sample.[42,149] Additionally the on-ice aerosol INP from July 28 was not active at T $\geq$ −15 °C, suggesting the aerosol INP was not influenced by meltwater on this day (see **Section 3.5.2**).

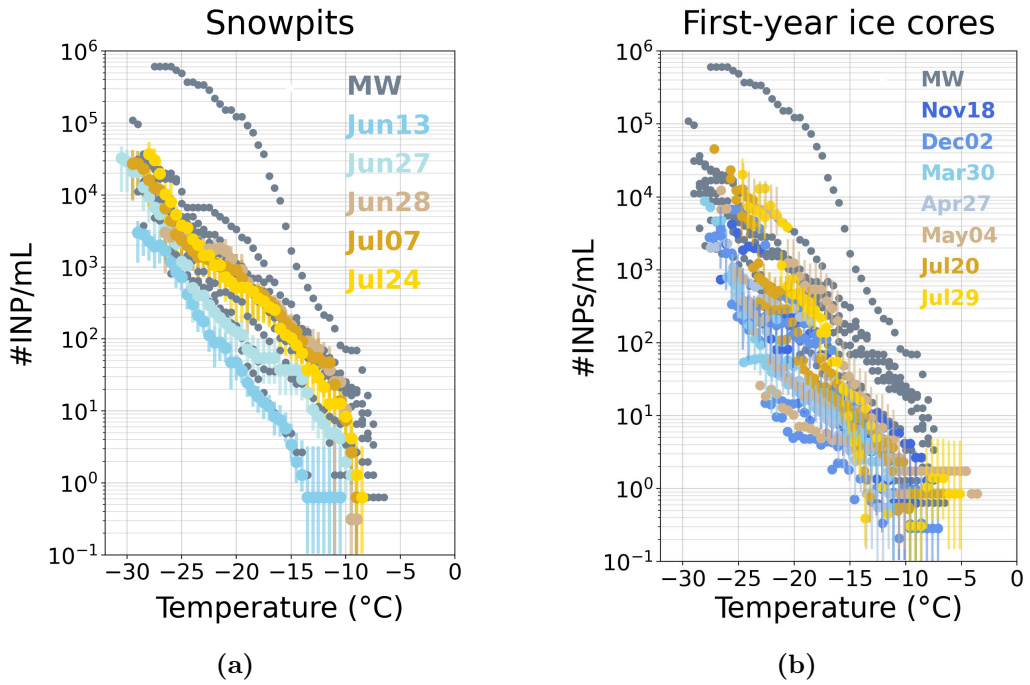

Figure 3.4: Comparison spectra of cumulative INP concentrations between meltwater (gray) and snow and first year sea ice (multi-color; left, right).

The relatively warm freezing temperatures and concentrations for the meltwater INPs shown in **Figure 3.3** illustrate a distinction between the BSW within the Arctic Ocean upper mixed layer and surface meltwater as INP sources, likely driven by distinct microbiological communities in the marine[150,151] versus sea ice[65,152] ecosystems. This microbial distinction between BSW, meltwater, and their interface was observed in those water layers from a lead sampled in July 2020 during MOSAiC.[42] The findings suggest a time-dependent community partitioning towards organisms capable of acclimatizing to the hyposaline conditions in the meltwater[153] in addition to increased quantities of dissolved organic matter[154] resulting from the release of photoprotective substances[155] under the high UV conditions in above-ice melt layers. **Figure 3.3** shows a general increase in meltwater INP over time, suggesting a link between the above-mentioned biological adaptations to low-saline environments and IN activity.

We would expect the microbiological composition of meltwater would be driven by the relative contributions of sea ice and snow melt[156] considering the unique compositions of

cryospheric ecology[65,66,157,158] within each melt source. The distinct influences of snow versus sea ice on the meltwater INPs is considered in **Figure 3.4**, which shows INP spectra for select snowpit and ice core samples compared to the meltwater samples. The snowpits from late June and July exhibited the closest similarity to average meltwater samples. The June 13 snowpit and July 4 meltwater spectra showed remarkable alignment between −13.5 to −20 °C, suggesting an at least partial shared INP population. The ice cores showed a depth-resolved variability in INP and were generally lower in INPs active at T ≥ −15 °C compared to the snow and meltwater samples. For surface melt ponds (opposed to under ice meltwater, which was not sampled), the melt of the snowpack on top of the sea ice is initiated first,[156] becoming the initial component of a melt pond in which the snow biology may have more time to establish itself as the dominant ice nucleating species. Nomura, et al (2023)[159] found that a meltwater layer in a lead sampled late summer (August 29) was predominantly sea ice melt, suggesting that the composition of meltwater on sea ice and leads may undergo a shift from a snowpack to sea ice influence. Furthermore, the different concentrations of biological INPs within frozen ice cores and meltwater may be due to the behavior of microbes living in frozen ice versus released into meltwater. Unfortunately, no meltwater samples from the Leg 4 floe were collected after July 28. Zeppenfeld, et al (2019)[148] reported on an enrichment in free glucose (a chemical marker potentially linked to ice nucleation activity) in water (BSW and surface microlayer) sampled from melt ponds and the marginal ice zone compared to the ice-free ocean and lead water, further suggesting that Arctic snow and sea ice may be significant reservoirs of biological INPs.

3.4 Comparing local meltwater and aerosol INP spectra

This section compares the INP spectra and composition of sample pairs collected at each ice station, consisting of a meltwater source and a down-wind on-ice aerosol filter sample (see

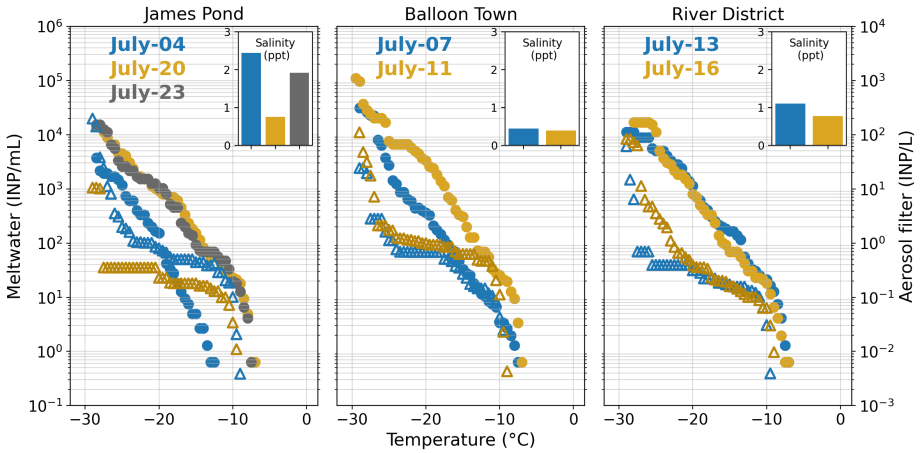

Figure 3.5: Comparison of cumulative INP spectra between on-ice aerosol filter samples (triangles) and upwind meltwater samples (circles) from ice station locations: James Pond, Balloon Town, and River District. Blue, gold, and gray distinguish both aerosol filter and meltwater samples from older to newer, respectively. Salinities for each meltwater sample are displayed in the top right. INP axes are arbitrarily aligned to compare spectra shapes, not concentrations.

Figure 2.1), to investigate the potential for a highly localized influence on the near-surface INPs.

Qualitative INP comparisons for the paired sample spectra across ice stations (James Pond (JP), Balloon Town (BT), and River District (RD)) are shown in **Figure 3.5**. For each of these pairs the meltwater source was sampled twice, resulting in three total meltwater sources sampled over time. This presents an opportunity to assess how the ice nucleating capacity of a meltwater source may change over time. Broadly, **Figure 3.5** shows the spectral shapes between both sample types (meltwater and on-ice aerosol) had similar slopes at the warmest and the coldest temperatures. The slopes between both sample types were typically aligned from the onset temperature to about −10 to −15 °C. After this temperature region, the slopes diverged. The aerosol spectra flattened whereas the meltwater spectra exhibited exponential growth. While the aerosol samples likely represent a mix of sources[50,57,59,63,24] present in the air, these results suggested meltwater may have a greater influence on the warm-temperature INPs detected on the aerosol filters versus other temperature ranges. This could occur via selective emission processes[160] for biological material capable of initiating freezing at those temperatures.

3.4.1 Meltwater INP temporal evolution

Regarding the general increase in meltwater INPs over the sample days, **Figure 3.5** presents a similar narrative to **Figure 3.4** with the additional context of distinguishing the samples into their distinct melt pond sources. The first meltwater sample at JP (July 4) displayed the lowest INP concentration across the meltwater samples. At JP over two weeks later (July 20), the meltwater INPs at T = −15 °C increased by one hundredfold and the onset freezing temperatures increased from T = −12.5 to −7.5 °C. The next meltwater source, temporally, was a melt pond near BT (July 7). Between the JP July 4 and BT July 7 samples, meltwater INPs were about 10x higher at T = −15 °C and onset temperatures were higher (−7.5 °C) at BT. The BT meltwater sample from July 11 had a greater INP concentration across the temperature range compared to the July 7 BT sample ($\sim$ 5x from −8 to −15 °C and $\sim$ 10x from −15 to −25 °C), similar to the evolution of INP in JP from July 4 to July 20. The evolution of INP within the same pond suggests processes responsible for the production of nucleating material: the continuation of melt which releases trapped sea ice microbes[65,161] and particulate matter sediment,[162] the growth of osmotically adapted communities seeded from the sea ice melt, or accumulation of INPs deposited from the air. Differences in INPs between the ponds may have been due to microbiological variability driven by pond morphology. This could have included sea ice thickness impacting the rate of melt pond formation and composition and number of microbiota within the ice. Additionally, melt pond area and depth could have impacted the absorption of photosynthetically active radiation. However, differences in INPs between the ponds became less distinct over time: The meltwater INPs had increasing concentrations and onset temperatures between the first and second meltwater sample pairs until mid-July. There was no significant difference in spectra between the RD meltwater INPs and the July 20 and July 23 JP meltwater INPs. This mid-July observation aligned with the peak in weekly average rate of surface ice melt (July 16).[122] After this point, early season variability in pond microbiology driven by

inhomogeneous pond morphology likely decreased, and the INPs in the meltwater became less distinguishable between ponds over time.

3.4.2 Inferences to a regional meltwater influence on atmospheric INPs

Regarding the on-ice aerosol, all samples exhibited similar spectral shapes (**Figure A.4**). However, the spectral slopes varied in their alignment with the associated meltwater sample pair, suggesting the meltwater influence is not constant across the air filter samples. For INPs active at T ≥ -17.5 °C, the meltwater and on-ice aerosol sample pair from July 7 aligned remarkably well. In contrast on July 11, the sample pairs aligned only from -10 to -12 °C, in which the on-ice aerosol filter also displayed a relative enhancement in INP compared to July 7. The spectral slopes between sample types at the RD station diverged at a warmer temperature than for the JP and BT samples (near -10 °C versus < -15°C). This suggests that if there was an INP influence from the highly localized meltwater upwind of these air filters, melt pond properties or atmospheric conditions drove a selective emission process for a smaller range of INPs, skewed towards higher temperatures. A large drainage event on July 11-13 decreased the in-situ melt pond areal fraction from 21 to 15 %[113] and the 1x1 degree melt pond areal fraction centered on the *Polarstern* from 33 to 29% (**Figure 3.1**). This may have reduced the overall emissions from local ponds, driving the spectral divergence seen in the RD panel of **Figure 3.5**. The spectral slopes of the JP on-ice aerosol align with the meltwater samples taken July 20 and July 23 between -8 to -15 °C. While the meltwater INPs at JP underwent a temporal shift to warmer temperatures, the on-ice aerosol sample on July 4 was already displaying similar spectral characteristics to the later meltwater samples at JP. This suggests that despite the relative proximity to JP, the on-ice aerosol INPs at this site may have been influenced more strongly by a regional meltwater INP signature versus a single pond.

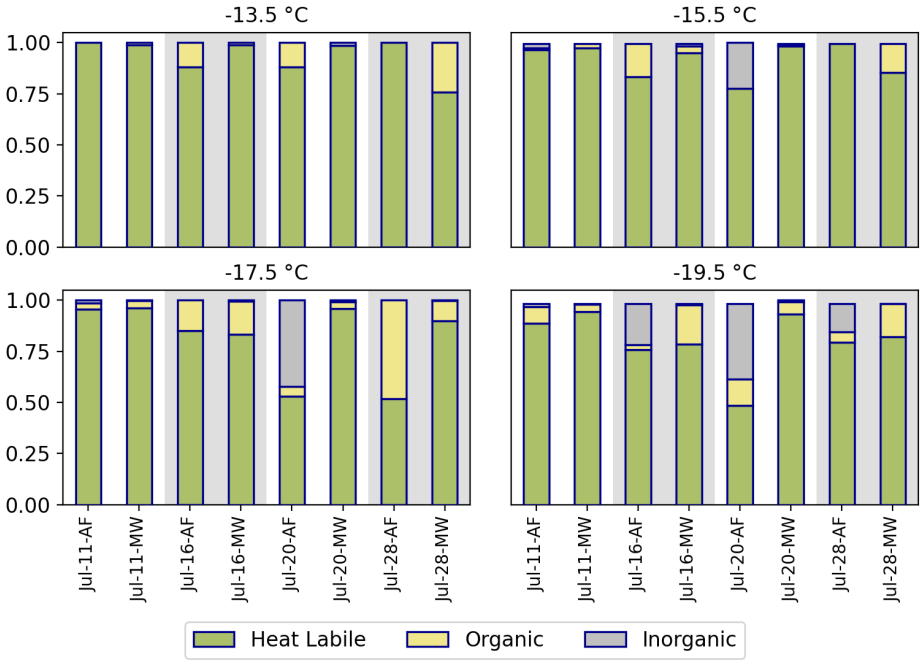

Figure 3.6: Relative fraction of heat labile, organic, and inorganic INPs at -13.5, -15.5, -17.5, and -19.5 °C for select co-located meltwater and on-ice aerosol filter samples. Sample identifiers with "-MW" are meltwater samples and those with "-AF" are aerosol filters.

Figure 3.6 shows heat and peroxide treatment results for a subset of co-located ice station sample pairs. The meltwater INP composition for each treated sample was almost totally biological at −13.5 °C, with the exception of July 28 (the singular meltwater sample taken from a lead) in which the fractions of biological and organic material were 0.76 and 0.24, respectively. The on-ice aerosol INP compositions were also predominantly biological at −13.5 °C, with organic fractions of 12 % for July 16 and July 20. No inorganic (i.e., likely mineral) INPs were observed above detection limits at this temperature for either sample type. Note, −13.5 °C was the highest common temperature in which heat stable (organic and inorganic) INPs were detected across treated samples, a value necessary for computing the comparative fractions for each type (**Figure A.6**). Heat-stable INPs were generally undetected above −13.5 °C, suggesting that the INPs in both the on-ice aerosol and meltwater samples were predominantly biological above this temperature. The heat labile fractions typically decreased with decreasing temperature, however an exception to this occurred for the July 11 sample in which the inorganic (biological) percent remained ≤ 2 %

($\geq 90\,\%$) across temperatures. Additionally, only trace inorganic fractions were detected in the meltwater samples. This suggests that meltwater was not a source of inorganic INPs.

Furthermore, the on-ice aerosol INP compositions shifted from predominantly biological to more diverse at colder temperatures. These observations suggest a selective emissions process for biological INP active at $T \geq -15.5\,°C$. There is evidence of covariance between on-ice aerosol INP concentrations between -10 and $-20\,°C$ and wind speed above about 3 m/s (**Figure A.7a**). Bubble bursting may preferentially emit biological material due to the scavenging of particles[73] or greater partitioning of surface active exopolymeric secretions of microalgae and bacteria[72] on the bubble surface. However, melt ponds are characteristically different from the open ocean given their shallow depths, limited fetch, and low salinity. Thus, a wind-speed dependent emissions process such as investigated for SSA from the open ocean or in coastal zones[76,163] may not directly apply to individual ponds. Instead, a larger ponded area, where the meltwater fetch is more extensive, might be required for such processes to have a meaningful effect on INP emissions. Enhanced film droplet generation at wind speeds < 5 m/s observed by Leck, et al (2002)[164] suggest the existence of non-wind driven bubble mechanisms, such as the release of trapped bubbles during the melting of sea ice[77] or biological respiration. There are many studies[165,166,167] investigating the differences in wind-driven bubble bursting processes for fresh versus saline water. However, more work needs to be done regarding non-wind driven differences in bubble formation and size distributions across salinity gradients to understand emissions from melt ponds.

3.5 Linking the aerosol INPs downwind of melt ponds to the broader Arctic region

3.5.1 Comparison of on-ice versus on-board aerosol INPs

Figure 3.7 shows that the rain-free on-ice filter INP concentrations were within the range defined by the INP concentrations of the aerosol filters deployed on the *Polarstern* for the

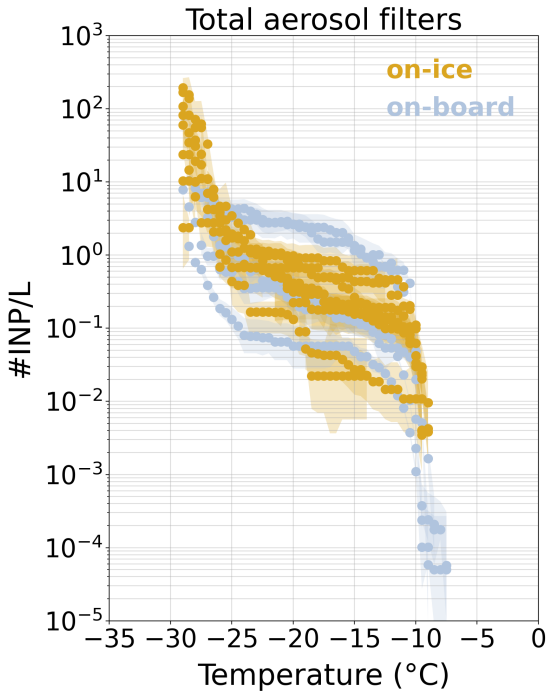

Figure 3.7: Cumulative concentrations of INP collected on aerosol filters deployed on the ice, downwind of open water sources - excluding July 2 (gold) and on the P-deck of *Polarstern* (blue) with shading denoting the 95% confidence intervals.

month of July 2020. The agreement indicates a shared INP influence within the vertical and horizontal span (see Figure A.1) of the two sampling locations, with differences at the warm end of the temperature spectrum attributable to sample volumes, which determine detection limits. The on-ice filters did not collect INPs capable of nucleating ice at temperatures as high as detected on the on-board filters (-7.2°C), likely due to the much larger total volumes of air collected during continuous 3-day sampling periods, making on-board filters more capable of capturing statistically rare, warm-temperature INPs (**Figure A.2**). The similarity between both aerosol filter sample types further suggests that the potential influence of meltwater on the near-surface aerosol filters is likely regional, overshadowing any impact from an individual pond.

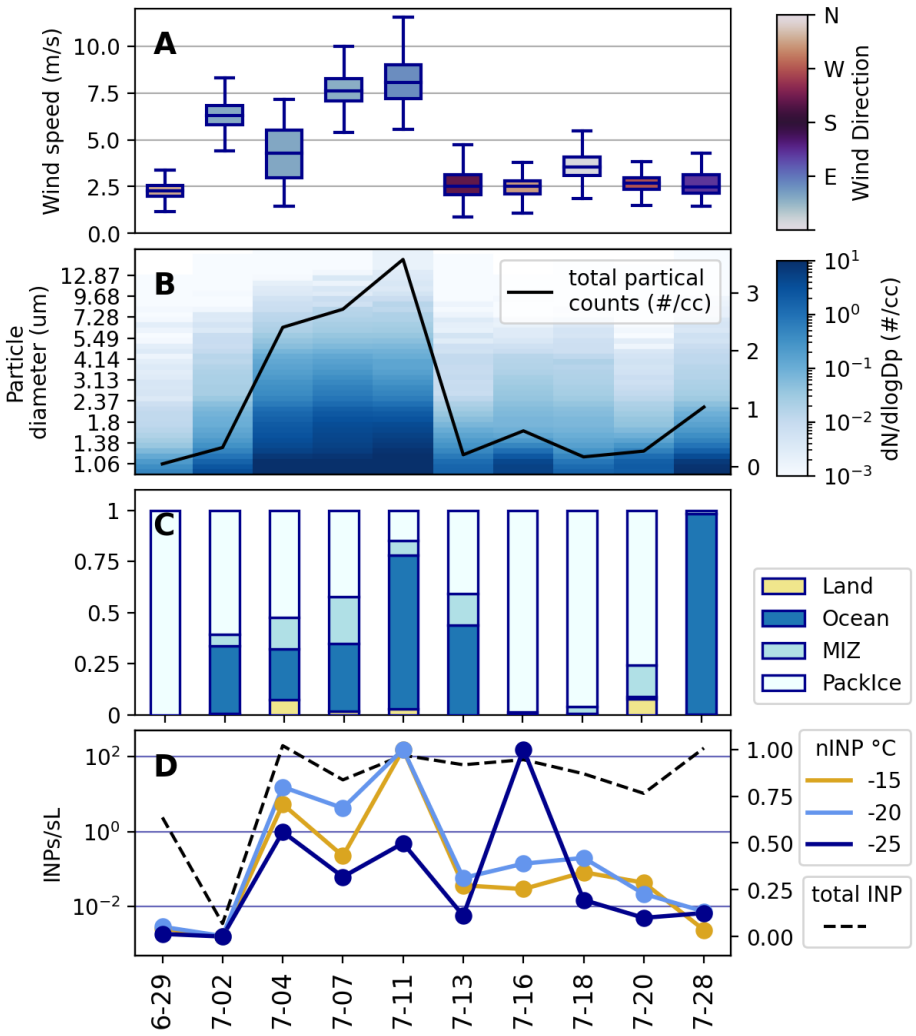

Figure 3.8: A) Box plots show the median (line), interquartile range (box), and 1.5xIQR (whiskers) 1-min wind speeds measured by the Met City meteorological tower 2 m above the surface, colored by the daily median 1-min, 2 m wind directions. B) Heat map shows daily-averaged 1-min dN/dlogDp as measured by the APS. The black line (right-axis) shows the total particle counts. C) The bars show the relative areal fraction of surface type (designated by MASAM2 Sea Ice Concentration product) passed over by FLEXPART simulated 1-day 100 m air mass. D) (Black dash) Total INP concentration (INPs/sL). (Colors) Normalized INP concentrations (nINP) by the maximum concentration across samples at select temperatures (−15, −20, −25 °C).

3.5.2 Linking aerosol filter INPs to air masses

In this section, we investigated the potential meltwater influence on near-surface aerosol INPs by considering local meteorological conditions and air mass transport history. **Figure 3.8** shows **(A)** the daily wind speed and direction, **(B)** daily-averaged supermicron particle size distributions and total particle counts, and **(C)** fractions of surface types in which the 1-day FLEXPART air mass trajectories passed over during each sampling day (the surface types relevant for meltwater are pack ice and MIZ). Panel **(D)** shows values of INPs normalized by the maximum observed INP level within each temperature range. We utilized this metric to show intersample variation in INPs at "warm" (−15 °C), "middle" (−20 °C), and "cold" (−25 °C) temperatures to represent how different populations of INPs may vary as local conditions change, revealing potentially distinct sources.

3.5.2.1 High wind gradients from over mixed sources influence aerosol INPs

Figure 3.8 shows covariance between warm, middle, and cold INP populations during a period (July 4 - July 11) of high easterly winds (medians = 4.3, 7.6, 8.1 m/s; maxima = 7.2, 10.8, 11.6). This period corresponds to the highest values of supermicron particle counts **(B)** and warm and middle INP populations across the samples **(D)**. While July 2 also had high easterly winds, precipitation likely caused the decrease in supermicron particles and aerosol INP via wet scavenging (see **Section 3.2**, **Figure A.5**). Total INP concentration peaked on July 4, but the warm and middle INP populations reached their highest values on July 11. This might have been due to the on-ice sampling period taking place during the maximum wind speeds on July 11 (**Figure A.2**). There is evidence of a greater correlation (r^2 = 0.51, 0.43) between daily-average wind speed and INP concentration at −20 and −15°C (**Figure A.7a**) which suggests that at certain temperatures, INPs were more sensitive to wind-driven selective emission processes. The 1-day trajectories traveled over a mix of surfaces during this period **(C)**. Given the higher wind speeds, the path the air mass took up to 7 days prior (**Figure A.9**) may be more representative of the air reaching the on-ice aerosol sampler than a 1-day trajectory. Figure **A.8** shows similar fractions of surface types beneath

the 7-day trajectories during the July 4-11 period, indicating common sources during this period. Wind-driven bubble-bursting over open water (ice-free ocean or meltwater present in leads and ponds in the pack ice or MIZ) may be responsible for the enhancement of warm temperature INPs due to the partitioning of biogenic particles on the bubble surface.[72,73] The higher warm and middle nINP compared to the cold nINP during this high wind period shown in **Figure 3.8D** emphasizes this implication. Sea spray typically lacks the warmer-temperature INPs unless over biologically active ocean regions.[99,129] Although the sea water at 11 m reached maximum chlorophyll-*a* levels (a proxy for biological activity[168]) during July 2020,[56] warm-temperature INPs were not detected on an on-ice aerosol sample with a predominant marine influence (discussed in **Section 3.5.2**). This does not entirely discount a source of warm INPs from the ice-free ocean. In addition to generating aerosols from bubble-bursting from meltwater, winds over the pack ice may re-emit sea spray aerosol from blowing snow.[169,170] However, the wet surface due to melting ice and snow during summer makes blowing snow events more relevant for winter aerosol populations,[171] thus supporting emission processes across the water-air interface.

July 13 had much lower wind speeds than the previous sample days (medians: 2.5 m/s; maxima: 5.4 m/s) and a covarying decrease in all populations of nINP, total INP, and supermicron concentration (**Figures 3.2 & 3.8B, D**). These lower particle counts may be attributed to the cessation of high wind speeds in addition to a predominant wind direction from the south **(A)** in which the 1-day trajectory traveled over a mix of surface types (ocean, MIZ, pack ice = 0.44, 0.16, 0.41) **(C)**. Low winds over a high fraction of ice-free ocean may have driven the low INP concentrations on this day due to reduced wind-driven emissions in addition to a suppression of the potential meltwater influence by insufficient residence time over pack ice.

3.5.2.2 Low winds from over the pack ice influence warm INPs

The low total INPs on June 29 **(D)** can be attributed to the low melt pond fraction (**Figure 3.1**, **Section 3.2**) and wind speeds **(A)**. Cold temperature INPs reached their

maximum levels across samples on July 16 whereas the warm INP population experienced a relative decrease. The middle INP population increased slightly but remained at relatively similar concentrations to the other samples. These observations suggest the cold INP population was influenced by a distinct source. Total INP and supermicron particles experienced a slight increase on July 16, however, the supermicron concentration did not correlate with warm and middle INP populations as was observed during the high wind period. No increase in submicron particle counts occurred (**Figure A.9**), suggesting the distinct INP source was not within this size regime. **Figure A.3** shows a strong northerly 1-day trajectory with little to no influences from surface types other than the pack ice, yet the source of cold INP enhancement from northern latitudes is currently unclear. Between July 16 and July 18 the total INP, supermicron and submicron particle counts decreased (**Figures 3.8 & A.9**). The cold INP population also experienced a decrease, however the warm and middle INP populations increased relative to the other sample days. Both July 16 and 18 had winds generally from the north or northwest, with large fractions of pack ice influence (0.99, 0.96). However, the higher wind speeds that occurred on July 18 (median = 3.5 m/s; max = 5.6 m/s) may be responsible for the relative increase in warm and middle INPs, similar to what was observed during the high wind period. Given the absence of open ocean influence on the 1-day trajectories, July 18 suggests a condition where strong winds from over the pack ice and MIZ drove an enhancement in warm temperature INPs, potentially attributed to the meltwater from ponds or leads. July 20 showed similar conditions to July 18 with lower, more westerly winds with a larger influence from the MIZ and land (0.15, 0.08) in which the intersample trend in warm, middle, and cold INPs was negative compared to the previous sample day, potentially attributable to the lower wind speeds over a lower pack ice fraction.

3.5.2.3 Transport from over ice-free ocean leads to a distinct INP population

The sample on July 28 was distinguished by low, southerly winds **(A)** from over the ice-free ocean (ocean surface fraction = 0.98) **(C)** and an increase in total super- and sub-micron particle counts (**B**, **Figure A.9**). Total INP increased **(D)**, however the warm, middle, and

cold INP populations were low, indicating the spike in total INP was due to INPs active at T $< -25\,^{\circ}$C. The INP spectrum for this sample (**Figures A.4** & **A.6a**) resembled one characterized as marine organic in McCluskey, et al. (2018)[129] (Fig5d). Over the northern Atlantic, they found that INPs did not freeze at T $\geq -15\,^{\circ}$C and were heat stable (contained organic material). Despite the low wind speeds (median, max: 2.5, 4.3 m/s), the fetch over the ice-free ocean was likely great enough to entirely influence the on-ice aerosol INP. The meltwater sampled on July 28 (**Figure 3.3**), which contained the second-highest amount of INPs for the meltwater samples across all temperatures, suggests the on-ice aerosol was not influenced by a potential local meltwater source on this day.

3.5.2.4 Synthesis

This analysis indicated that variability in near-surface INPs (those active at T $\geq -25\,^{\circ}$C) were primarily driven by wind speed, in which the warm and middle INP populations experienced a stronger wind speed dependence. Correlations between wind speed and supermicron particle counts were also observed (**Figure 3.8B**) aligning with other studies in marine Arctic environments, particularly over open ocean and leads.[76,163,164,172] With the exception of June 29 and July 2 (due to ice lid formation) melt pond fractions between 30 - 40 % were observed for all sample days (**Figure 3.1**), suggesting a near-constant source of INPs from regional melt ponds, and other reservoirs of meltwater.[42] The INPs within each melt pond increased over time and trended towards homogeneity, suggested by a convergence in the meltwater INP spectra (**Figures 3.3 & 3.5**). Under these conditions, it is suggested that the relevant in-situ melt pond statistics[42] (**Section 3.1.2**) for on-ice aerosol INP are fetch-related, such as melt pond area. The agreement between the on-board aerosol INPs, in which longer sampling periods represent an accumulation of INPs from potentially more diverse sources, and the on-ice aerosol INPs (**Figure 3.7**) further suggests that an influence from meltwater was not solely from the upwind meltwater source but from a wider area. Boundary layer conditions such as height and vertical mixing (**Figures A.10 & A.11**) were also

considered as an influence on on-ice aerosol INPs and discussed briefly in the Supplemental Information **Section A.2**, but covariability with INP concentrations was not observed.

Chapter 4

Conclusions and Broader Impacts

We presented observations from July 2020 of INP concentrations and temperature spectra from aerosol filter samples located on the ice downwind of meltwater features and on-board *Polarstern*, and compared with the spectra observed in source samples of meltwater, snow, ice cores, and bulk sea water. INPs active at T ≥ -10 °C were detected for 80 % of the on-ice aerosol filters. The detection of warm-temperature, biological INPs in summer (July) for on-ice aerosol samples aligned with previous work on the annual cycle of INP observations in this region[56] that showed a distinct summertime peak that was potentially related to the high fractions of hyperfluorescent aerosol measured in June.[132] The similarities between the ship-based and on-ice aerosol filters suggested a regional meltwater signature, rather than a strong influence from individual melt ponds. The variability in INP concentrations on the on-ice aerosol was attributed to coarse-mode aerosol scavenging by precipitation and wind speed. These findings further emphasize that the potential meltwater influence is regional, in which an accumulation of ponded surfaces traveled over by an air mass is more likely to contain biological, warmer temperature INPs via selective, wind-driven emissions processes.

INP concentrations in meltwater samples were about 10-fold higher than those in BSW and 90 % of samples contained INPs capable of freezing at T ≥ -10 °C, except for the earliest meltwater sample. The similarities between the snow and meltwater INP spectra were greater than between the ice core and meltwater spectra. However, the temporal increase in INP concentrations at all temperatures (within the same melt pond) can be attributed to the release of additional INPs from the ice as melt progressed and may suggest melt ponds are a unique habitat[42] for growth of osmotically adapted organisms from the ice that may act as INPs. Many cryospheric organisms contain specific cold-environment adaptations such as ice-binding proteins[68,69] that are, by nature, highly ice-active. Future

work is needed to determine whether the ice nucleation capacity of materials within meltwater can be attributed to specific organisms, proteins, or organic compounds.

The INP spectra for the meltwater sources and on-ice aerosol samples shared similar slopes at T $\geq -15\,^{\circ}$C, suggesting the meltwater samples contained INPs that could influence the airborne INP concentrations that were active at those temperatures. Additionally, heat and peroxide treatments on the meltwater and on-ice aerosol samples indicated INPs were mostly biological up to $-19.5\,^{\circ}$C. Higher compositional diversity in the on-ice aerosol INPs with decreasing temperature, compared to the meltwater samples, suggested a selective emissions process for heat-labile INP material as well as the likelihood of other sources influencing airborne INPs. For example, inorganic INPs were detected in the aerosol samples, but not in the meltwater source samples.

The conditions present during July 2020 were especially relevant for potential cloud impacts. The latter-half of July 2020 experienced a high frequency of low-clouds (**Figure A.10**) likely associated with record mean temperature and moisture in July,[95] in which climate change may drive a continuation of these record-breaking conditions. Lonardi et al. (2021)[173] reported low amounts of cloud-ice present down to the surface during MOSAiC from July 19-21. The temperatures of ice-containing cloud tops in the lowest 2.5 km suggested ice formation at T > -15 or $-10\,^{\circ}$C. Furthermore, findings by Griesche et al. (2021)[174] showed evidence that heterogeneous ice formation above T $= -10\,^{\circ}$C in AMPCs occurred by a factor of $2-6$ times more often when the cloud layer was coupled to the surface. The evidence of biological INPs active at T $\geq -10\,^{\circ}$C on the on-ice aerosol sample on July 20 and variability in θ_e (a well-mixed below-cloud environment; **Figures 3.2, 3.6 & A.10**) suggests a potential influence from regional meltwater INPs within the clouds on this date. June 29, July 11, and July 18 were also characterized by low-clouds and low θ_e variance in addition to near-surface aerosol INPs active at T $\geq -10\,^{\circ}$C, suggesting these surface-cloud coupling relevant conditions were not singular.

This work established a similarity in warm-temperature, biological INPs between near-surface air and meltwater. However, more measurements of INPs in the air and in the meltwater during the melt season are necessary in order to untangle what drives variations in this influence. Ideally, daily aerosol and source samples collected from before melt until deep into the melt season could document potential differences in the aerosol INP spectra as a function of melt season progression. Biological characterization (DNA sequencing) of meltwater and aerosol INPs would also be useful for elucidating whether primary production within meltwater is a factor in the temporal increase in meltwater INP over time, and whether similar taxa were found in the air. A key question that remains is identifying the emission mechanism(s) responsible for aerosolizing INPs from meltwater, which would aid in understanding the driving factor behind the meltwater's influence on aerosol INP levels. Aerosol flux measurements over several melt ponds as they form and evolve may reveal distinctions between wind and non-wind driven emission mechanisms such as those driven by the thermodynamics of melting sea ice or the release of gas from biology within the ponds. Aerosol flux measurements could be carried out using a relaxed eddy accumulation system as described in Gaman (2004),[175] configured to sample aerosols of a relevant size for INPs from over melt ponds.

Bibliography

[1] S. Cassotta C. Derksen A. Ekaykin A. Hollowed G. Kofinas A. Mackintosh J. Melbourne-Thomas M.M.C. Muelbert G. Ottersen H. Pritchard M. Meredith, M. Sommerkorn and E.A.G. Schuur. *Polar Regions*, pages 203–320. Cambridge University Press, 2019.

[2] Mika Rantanen. The arctic has warmed nearly four times faster than the globe since 1979 communications earth & environment, 2022.

[3] Mark C Serreze and Roger G Barry. Processes and impacts of arctic amplification: A research synthesis. *Global and Planetary Change*, 77:85–96, 5 2011.

[4] Alex Hall. The role of surface albedo feedback in climate. *Journal of Climate*, 17:1550–1568, 4 2004. Publisher: American Meteorological Society Section: Journal of Climate.

[5] James A Screen and Ian Simmonds. The central role of diminishing sea ice in recent arctic temperature amplification. *Nature*, 464:1334–1337, 4 2010. Publisher: Nature Publishing Group.

[6] Intergovernmental Panel on Climate Change (IPCC), editor. *The Earth's Energy Budget, Climate Feedbacks and Climate Sensitivity*, pages 923–1054. Cambridge University Press, 2023.

[7] Matthew D Shupe and Janet M Intrieri. Cloud radiative forcing of the arctic surface: The influence of cloud properties, surface albedo, and solar zenith angle. *Journal of Climate*, 17:616–628, 2 2004. Publisher: American Meteorological Society Section: Journal of Climate.

[8] Ivy Tan, Trude Storelvmo, and Mark D Zelinka. Observational constraints on mixed-phase clouds imply higher climate sensitivity. *Science*, 352:224–227, 4 2016. Publisher: American Association for the Advancement of Science.

[9] Stefan Hofer, Lily C Hahn, Jonah K Shaw, Zachary S McGraw, Olimpia Bruno, Franziska Hellmuth, Marianne Pietschnig, Idunn Aa Mostue, Robert O David, Tim Carlsen, and Trude Storelvmo. Realistic representation of mixed-phase clouds increases projected climate warming. *Communications Earth Environment*, 5:1–12, 7 2024. Publisher: Nature Publishing Group.

[10] Hugh Morrison, Gijs de Boer, Graham Feingold, Jerry Harrington, Matthew D Shupe, and Kara Sulia. Resilience of persistent arctic mixed-phase clouds. *Nature Geoscience*, 5:11–17, 1 2012. Publisher: Nature Publishing Group.

[11] Alexander V Matus and Tristan S L'Ecuyer. The role of cloud phase in earth's radiation budget. *Journal of Geophysical Research: Atmospheres*, 122:2559–2578, 2017.

[12] James O Pinto. Autumnal mixed-phase cloudy boundary layers in the arctic. *Journal of the Atmospheric Sciences*, 55:2016–2038, 6 1998. Publisher: American Meteorological Society Section: Journal of the Atmospheric Sciences.

[13] Hugh Morrison, Matthew D Shupe, James O Pinto, and Judith A Curry. *Geophysical Research Letters*, 32, 2005.

[14] Jerry Y Harrington, Tamir Reisin, William R Cotton, and Sonia M Kreidenweis. Cloud resolving simulations of arctic stratus: Part ii: Transition-season clouds. *Atmospheric Research*, 51:45–75, 4 1999.

[15] Amy Solomon. Acp - the relative impact of cloud condensation nuclei and ice nucleating particle concentrations on phase partitioning in arctic mixed-phase stratocumulus clouds, 2018.

[16] T Mauritsen, J Sedlar, M Tjernström, C Leck, M Martin, M Shupe, S Sjogren, B Sierau, P O G Persson, I M Brooks, and E Swietlicki. An arctic ccn-limited cloud-aerosol regime. *Atmospheric Chemistry and Physics*, 11:165–173, 1 2011. Publisher: Copernicus GmbH.

[17] Zieger P. Ekman Schmale, J. Aerosols in current and future arctic climate. *Nat. Clim. Chang.*, 11:95–105, 2021.

[18] Gregory Cesana and Trude Storelvmo. Improving climate projections by understanding how cloud phase affects radiation. *Journal of Geophysical Research: Atmospheres*, 122:4594–4599, 2017.

[19] T. Uttal C. N. Long M. D. Shupe R. S. Stone Cox, C. J. and S. Starkweather. The role of springtime arctic clouds in determining autumn sea ice extent in: Journal of climate volume 29 issue 18 (2016). *Journal of Climate*, page 6581–6596, 2016.

[20] Matthew D.;Perovich Don;Solomon Amy; Persson, P. Ola G.;Shupe. Linking atmospheric synoptic transport, cloud phase, surface energy fluxes, and sea-ice growth: observations of midwinter sheba conditions climate dynamics. *Climate Dynamics*, 49:1341–1364, 2016.

[21] Barahona D. Coopman Q Tan, I. Potential link between ice nucleation and climate model spread in arctic amplification. *Geophysical Research Letters*, 2022.

[22] M. Stengel Philipp, D. and B. Ahrens. Analyzing the arctic feedback mechanism between sea ice and low-level clouds using 34 years of satellite observations. *Journal of Climate*, 33:7479–7501, 2020.

[23] Piyush Jain, Quinn E Barber, Steve Taylor, Ellen Whitman, Dante Castellanos Acuna, Yan Boulanger, Raphaël D Chavardès, Jack Chen, Peter Englefield, Mike Flannigan, Martin P Girardin, Chelene C Hanes, John Little, Kimberly Morrison, Rob S Skakun, Dan K Thompson, Xianli Wang, and Marc-André Parisien. Canada under fire – drivers and impacts of the record-breaking 2023 wildfire season.

[24] V G Bondur, I I Mokhov, O S Voronova, and S A Sitnov. Satellite monitoring of siberian wildfires and their effects: Features of 2019 anomalies and trends of 20-year changes. *Doklady Earth Sciences*, 492:370–375, 2020.

[25] Christina S McCluskey, Paul J DeMott, Anthony J Prenni, Ezra J T Levin, Gavin R McMeeking, Amy P Sullivan, Thomas C J Hill, Shunsuke Nakao, Christian M Carrico, and Sonia M Kreidenweis. Characteristics of atmospheric ice nucleating particles associated with biomass burning in the us: Prescribed burns and wildfires. *Journal of Geophysical Research: Atmospheres*, 119:10458–10470, 2014.

[26] Anthony J Prenni, Paul J DeMott, Amy P Sullivan, Ryan C Sullivan, Sonia M Kreidenweis, and David C Rogers. Biomass burning as a potential source for atmospheric ice nuclei: Western wildfires and prescribed burns. *Geophysical Research Letters*, 39, 2012.

[27] Hill T. C. J. Levin E. J. T. Twohy C. H. Moore K. A. Weller-Z. D. et al. Barry, K. R. Observations of ice nucleating particles in the free troposphere from western us wildfires. *Journal of Geophysical Research: Atmospheres*, 2021.

[28] R Engelmann, A Ansmann, K Ohneiser, H Griesche, M Radenz, J Hofer, D Althausen, S Dahlke, M Maturilli, I Veselovskii, C Jimenez, R Wiesen, H Baars, J Bühl, H Gebauer, M Haarig, P Seifert, U Wandinger, and A Macke. Wildfire smoke, arctic haze, and aerosol effects on mixed-phase and cirrus clouds over the north pole region during mosaic: an introduction. *Atmospheric Chemistry and Physics*, 21:13397–13423, 2021.

[29] Yutaka Tobo, Kouji Adachi, Paul J DeMott, Thomas C J Hill, Douglas S Hamilton, Natalie M Mahowald, Naoko Nagatsuka, Sho Ohata, Jun Uetake, Yutaka Kondo, and Makoto Koike. Glacially sourced dust as a potentially significant source of ice nucleating particles. *Nature Geoscience*, 12:253–258, 4 2019. Publisher: Nature Publishing Group.

[30] Kevin R Barry, Thomas C J Hill, Marina Nieto-Caballero, Thomas A Douglas, Sonia M Kreidenweis, Paul J DeMott, and Jessie M Creamean. Active thermokarst regions

contain rich sources of ice-nucleating particles. *Atmospheric Chemistry and Physics*, 23:15783–15793, 12 2023. Publisher: Copernicus GmbH.

[31] Kevin R Barry, Thomas C J Hill, Kathryn A Moore, Thomas A Douglas, Sonia M Kreidenweis, Paul J DeMott, and Jessie M Creamean. Persistence and potential atmospheric ramifications of ice-nucleating particles released from thawing permafrost. *Environmental Science Technology*, 57:3505–3515, 3 2023. Publisher: American Chemical Society.

[32] Julienne Stroeve and Dirk Notz. Changing state of arctic sea ice across all seasons. *Environmental Research Letters*, 13:103001, 9 2018. Publisher: IOP Publishing.

[33] D. K. Perovich and C. Polashenski. Albedo evolution of seasonal arctic sea ice. *Geophysical Research Letters*, 2012.

[34] J. C Comiso. Large decadal decline of the arctic multiyear ice cover. *Journal of Climate*, 25:1176–1193, 2012.

[35] Ping Chen, Xiaoyu Wang, Jinping Zhao, Tao Li, Junqiang Shi, Fangyi Zong, and Lai Wei. Variability of arctic sea ice age and its relationship with atmospheric circulation patterns. *Frontiers in Marine Science*, 10, 11 2023.

[36] C Fowler, W J Emery, and J Maslanik. Satellite-derived evolution of arctic sea ice age: October 1978 to march 2003. *IEEE Geoscience and Remote Sensing Letters*, 1:71–74, 4 2004.

[37] Zhenxia Long and Will Perrie. Air-sea interactions during an arctic storm. *Journal of Geophysical Research: Atmospheres*, 117, 2012.

[38] James Morison, Ron Kwok, Cecilia Peralta-Ferriz, Matt Alkire, Ignatius Rigor, Roger Andersen, and Mike Steele. Changing arctic ocean freshwater pathways. *Nature*, 481:66–70, 1 2012. Publisher: Nature Publishing Group.

[39] Kevin R Arrigo and Gert L Van Dijken. Continued increases in arctic ocean primary production. *Progress in Oceanography*, 136:60–70, 8 2015.

[40] Kevin R Arrigo, Donald K Perovich, Robert S Pickart, Zachary W Brown, Gert L Van Dijken, Kate E Lowry, Matthew M Mills, Molly A Palmer, William M Balch, Frank Bahr, Nicholas R Bates, Claudia Benitez-Nelson, Bruce Bowler, Emily Brownlee, Jens K Ehn, Karen E Frey, Rebecca Garley, Samuel R Laney, Laura Lubelczyk, Jeremy Mathis, Atsushi Matsuoka, B Greg Mitchell, G W K Moore, Eva Ortega-Retuerta, Sharmila Pal, Chris M Polashenski, Rick A Reynolds, Brian Schieber, Heidi M Sosik, Michael Stephens, and James H Swift. Massive phytoplankton blooms under arctic sea ice. *Science*, 336:1408, 6 2012. Number: 6087.

[41] K. R. Arrigo and G. L. van Dijken. Secular trends in arctic ocean net primary production. *Journal of Geophysical Research*, 2011.

[42] Madison M Smith, Hélène Angot, Emelia J Chamberlain, Elise S Droste, Salar Karam, Morven Muilwijk, Alison L Webb, Stephen D Archer, Ivo Beck, Byron W Blomquist, Jeff Bowman, Matthew Boyer, Deborah Bozzato, Melissa Chierici, Jessie Creamean, Alessandra D'Angelo, Bruno Delille, Ilker Fer, Allison A Fong, Agneta Fransson, Niels Fuchs, Jessie Gardner, Mats A Granskog, Clara J M Hoppe, Mario Hoppema, Mario Hoppmann, Thomas Mock, Sofia Muller, Oliver Müller, Marcel Nicolaus, Daiki Nomura, Tuukka Petäjä, Evgenii Salganik, Julia Schmale, Katrin Schmidt, Kirstin M Schulz, Matthew D Shupe, Jacqueline Stefels, Linda Thielke, Sandra Tippenhauer, Adam Ulfsbo, Maria van Leeuwe, Melinda Webster, Masaki Yoshimura, and Liyang Zhan. Thin and transient meltwater layers and false bottoms in the arctic sea ice pack—recent insights on these historically overlooked features. *Elementa: Science of the Anthropocene*, 11:25, 9 2023.

[43] Rebecca Caitlin Frew, Daniel Feltham, David Schroeder, and Adam William Bateson. Toward a marginal arctic sea ice cover: changes to freezing, melting and dynamics.

The Cryosphere Discussions, pages 1–18, 6 2023. Publisher: Copernicus GmbH.

[44] J Browse, K S Carslaw, G W Mann, C E Birch, S R Arnold, and C Leck. The complex response of arctic aerosol to sea-ice retreat. *Atmospheric Chemistry and Physics*, 14:7543–7557, 7 2014. Publisher: Copernicus GmbH.

[45] H Struthers, A M L Ekman, P Glantz, T Iversen, A Kirkevåg, E M Mårtensson, Ø Seland, and E D Nilsson. The effect of sea ice loss on sea salt aerosol concentrations and the radiative balance in the arctic. *Atmospheric Chemistry and Physics*, 11:3459–3477, 4 2011. Publisher: Copernicus GmbH.

[46] Martí Galí, Martine Lizotte, David J Kieber, Achim Randelhoff, Rachel Hussherr, Lei Xue, Julie Dinasquet, Marcel Babin, Eric Rehm, and Maurice Levasseur. Dms emissions from the arctic marginal ice zone. *Elementa: Science of the Anthropocene*, 9:113, 7 2021.

[47] Caroline Leck and Cecilia Persson. Seasonal and short-term variability in dimethyl sulfide, sulfur dioxide and biogenic sulfur and sea salt aerosol particles in the arctic marine boundary layer during summer and autumn. *Tellus B: Chemical and Physical Meteorology*, 1 1996.

[48] Matteo Feltracco, Elena Barbaro, Clara J M Hoppe, Klara K E Wolf, Andrea Spolaor, Rose Layton, Christoph Keuschnig, Carlo Barbante, Andrea Gambaro, and Catherine Larose. Airborne bacteria and particulate chemistry capture phytoplankton bloom dynamics in an arctic fjord. *Atmospheric Environment*, 256:118458, 7 2021.

[49] K J Sanchez, B Zhang, H Liu, G Saliba, C.-L. Chen, S L Lewis, L M Russell, M A Shook, E C Crosbie, L D Ziemba, M D Brown, T J Shingler, C E Robinson, E B Wiggins, K L Thornhill, E L Winstead, C Jordan, P K Quinn, T S Bates, J Porter, T G Bell, E S Saltzman, M J Behrenfeld, and R H Moore. Linking marine phytoplankton

emissions, meteorological processes, and downwind particle properties with flexpart. *Atmospheric Chemistry and Physics*, 21:831–851, 2021.

[50] A Stohl. Characteristics of atmospheric transport into the arctic troposphere. *Journal of Geophysical Research: Atmospheres*, 111, 2006.

[51] P K Quinn, G Shaw, E Andrews, E G Dutton, T Ruoho-Airola, and S L Gong. Arctic haze: current trends and knowledge gaps. *Tellus B: Chemical and Physical Meteorology*, 59:99–114, 1 2007.

[52] Randolph D Borys. Studies of ice nucleation by arctic aerosol on agasp-ii. *Journal of Atmospheric Chemistry*, 9:169–185, 7 1989.

[53] David C Rogers, Paul J DeMott, and Sonia M Kreidenweis. Airborne measurements of tropospheric ice-nucleating aerosol particles in the arctic spring. *Journal of Geophysical Research: Atmospheres*, 106:15053–15063, 2001.

[54] J Browse, K S Carslaw, S R Arnold, K Pringle, and O Boucher. The scavenging processes controlling the seasonal cycle in arctic sulphate and black carbon aerosol. *Atmospheric Chemistry and Physics*, 12:6775–6798, 8 2012. Publisher: Copernicus GmbH.

[55] Eyal Freud, Radovan Krejci, Peter Tunved, Richard Leaitch, Quynh T Nguyen, Andreas Massling, Henrik Skov, and Leonard Barrie. Pan-arctic aerosol number size distributions: seasonality and transport patterns. *Atmospheric Chemistry and Physics*, 17:8101–8128, 7 2017. Publisher: Copernicus GmbH.

[56] Jessie M Creamean, Kevin Barry, Thomas C J Hill, Carson Hume, Paul J DeMott, Matthew D Shupe, Sandro Dahlke, Sascha Willmes, Julia Schmale, Ivo Beck, Clara J M Hoppe, Allison Fong, Emelia Chamberlain, Jeff Bowman, Randall Scharien, and Ola Persson. Annual cycle observations of aerosols capable of ice formation in central

arctic clouds. *Nature Communications*, 13:3537, 6 2022. Publisher: Nature Publishing Group.

[57] J M Creamean, J N Cross, R Pickart, L McRaven, P Lin, A Pacini, R Hanlon, D G Schmale, J Ceniceros, T Aydell, N Colombi, E Bolger, and P J DeMott. Ice nucleating particles carried from below a phytoplankton bloom to the arctic atmosphere. *Geophysical Research Letters*, 46:8572–8581, 2019.

[58] M Hartmann, K Adachi, O Eppers, C Haas, A Herber, R Holzinger, A Hünerbein, E Jäkel, C Jentzsch, M van Pinxteren, H Wex, S Willmes, and F Stratmann. Wintertime airborne measurements of ice nucleating particles in the high arctic: A hint to a marine, biogenic source for ice nucleating particles. *Geophysical Research Letters*, 47:e2020GL087770, 2020. e2020GL087770 10.1029/2020GL087770.

[59] Markus Hartmann, Xianda Gong, Simonas Kecorius, Manuela van Pinxteren, Teresa Vogl, André Welti, Heike Wex, Sebastian Zeppenfeld, Hartmut Herrmann, Alfred Wiedensohler, and Frank Stratmann. Terrestrial or marine – indications towards the origin of ice-nucleating particles during melt season in the european arctic up to 83.7°thinsp;n. *Atmospheric Chemistry and Physics*, 21:11613–11636, 8 2021. Publisher: Copernicus GmbH.

[60] A Held, I M Brooks, C Leck, and M Tjernström. On the potential contribution of open lead particle emissions to the central arctic aerosol concentration. *Atmospheric Chemistry and Physics*, 11:3093–3105, 4 2011. Publisher: Copernicus GmbH.

[61] Heike Wex, Lin Huang, Wendy Zhang, Hayley Hung, Rita Traversi, Silvia Becagli, Rebecca J Sheesley, Claire E Moffett, Tate E Barrett, Rossana Bossi, Henrik Skov, Anja Hünerbein, Jasmin Lubitz, Mareike Löffler, Olivia Linke, Markus Hartmann, Paul Herenz, and Frank Stratmann. Annual variability of ice-nucleating particle concentrations at different arctic locations. *Atmospheric Chemistry and Physics*, 19:5293–5311, 4 2019. Publisher: Copernicus GmbH.

[62] Tina Šantl Temkiv, Robert Lange, David Beddows, Urška Rauter, Stephanie Pilgaard, Manuel Dall'Osto, Nina Gunde-Cimerman, Andreas Massling, and Heike Wex. Biogenic sources of ice nucleating particles at the high arctic site villum research station. *Environmental Science Technology*, 53:10580–10590, 9 2019. Publisher: American Chemical Society.

[63] Gabriel Pereira Freitas, Kouji Adachi, Franz Conen, Dominic Heslin-Rees, Radovan Krejci, Yutaka Tobo, Karl Espen Yttri, and Paul Zieger. Regionally sourced bioaerosols drive high-temperature ice nucleating particles in the arctic. *Nature Communications*, 14:5997, 9 2023. Publisher: Nature Publishing Group.

[64] Kevin R. Barry. *Ice nucleating particles in the arctic: Measurement and source tracking.* PhD thesis, Colorado State University, 2024.

[65] Antje Boetius, Alexandre M Anesio, Jody W Deming, Jill A Mikucki, and Josephine Z Rapp. Microbial ecology of the cryosphere: sea ice and glacial habitats. *Nature Reviews Microbiology*, 13:677–690, 11 2015. Publisher: Nature Publishing Group.

[66] Aviaja L Hauptmann, Marek Stibal, Jacob Bælum, Thomas Sicheritz-Pontén, Søren Brunak, Jeff S Bowman, Lars H Hansen, Carsten S Jacobsen, and Nikolaj Blom. Bacterial diversity in snow on north pole ice floes. *Extremophiles*, 18:945–951, 11 2014.

[67] Philipp Assmy, Mar Fernández-Méndez, Pedro Duarte, Amelie Meyer, Achim Randelhoff, Christopher J Mundy, Lasse M Olsen, Hanna M Kauko, Allison Bailey, Melissa Chierici, Lana Cohen, Anthony P Doulgeris, Jens K Ehn, Agneta Fransson, Sebastian Gerland, Haakon Hop, Stephen R Hudson, Nick Hughes, Polona Itkin, Geir Johnsen, Jennifer A King, Boris P Koch, Zoe Koenig, Slawomir Kwasniewski, Samuel R Laney, Marcel Nicolaus, Alexey K Pavlov, Christopher M Polashenski, Christine Provost, Anja Rösel, Marthe Sandbu, Gunnar Spreen, Lars H Smedsrud, Arild Sundfjord, Torbjørn Taskjelle, Agnieszka Tatarek, Jozef Wiktor, Penelope M Wagner, Anette Wold, Har-

ald Steen, and Mats A Granskog. Leads in arctic pack ice enable early phytoplankton blooms below snow-covered sea ice. *Scientific Reports*, 7:40850, 2017.

[68] Johanna C Winder, William Boulton, Asaf Salamov, Sarah Lena Eggers, Katja Metfies, Vincent Moulton, and Thomas Mock. Genetic and structural diversity of prokaryotic ice-binding proteins from the central arctic ocean. *Genes*, 14:363, 2 2023. Number: 2 Publisher: Multidisciplinary Digital Publishing Institute.

[69] Aneta Białkowska, Edyta Majewska, Aleksandra Olczak, and Aleksandra Twarda-Clapa. Ice binding proteins: Diverse biological roles and applications in different types of industry. *Biomolecules*, 10:274, 2 2020. Number: 2 Publisher: Multidisciplinary Digital Publishing Institute.

[70] C Krembs, H Eicken, K Junge, and J W Deming. High concentrations of exopolymeric substances in arctic winter sea ice: implications for the polar ocean carbon cycle and cryoprotection of diatoms. *Deep Sea Research Part I: Oceanographic Research Papers*, 49:2163–2181, 2002.

[71] Edward Bigg and C Leck. The composition of fragments of bubbles bursting at the ocean surface. *Journal of Geophysical Research (Atmospheres)*, 113:11209, 9 2008.

[72] Caroline Leck and E Keith Bigg. Biogenic particles in the surface microlayer and overlaying atmosphere in the central arctic ocean during summer. *Tellus B: Chemical and Physical Meteorology*, 57, 1 2005.

[73] Lena Dubitsky, Oliver McRae, and James C. Bird. Enrichment of scavenged particles in jet drops determined by bubble size and particle position. *Phys. Rev. Lett.*, 30, 2023.

[74] S J Norris, I M Brooks, G de Leeuw, A Sirevaag, C Leck, B J Brooks, C E Birch, and M Tjernström. Measurements of bubble size spectra within leads in the arctic summer pack ice. *Ocean Science*, 7:129–139, 2 2011. Publisher: Copernicus GmbH.

[75] D C Blanchard and A H Woodcock. Bubble formation and modification in the sea and its meteorological significance. *Tellus*, 9:145–158, 1957.

[76] E D Nilsson and Ü Rannik. Turbulent aerosol fluxes over the arctic ocean: 1. dry deposition over sea and pack ice. *Journal of Geophysical Research: Atmospheres*, 106:32125–32137, 2001.

[77] J C Drake. Electrification accompanying the melting of ice particles. *Quarterly Journal of the Royal Meteorological Society*, 94:176–191, 1968.

[78] Małgorzata Stramska, Roman Marks, and Edward C Monahan. Bubble-mediated aerosol production as a consequence of wave breaking in supersaturated (hyperoxic) seawater. *Journal of Geophysical Research: Oceans*, 95:18281–18288, 1990.

[79] J C Stroeve, T Markus, L Boisvert, J Miller, and A Barrett. Changes in arctic melt season and implications for sea ice loss. *Geophysical Research Letters*, 41:1216–1225, 2014.

[80] Rebecca J Rolph, Daniel L Feltham, and David Schröder. Changes of the arctic marginal ice zone during the satellite era. *The Cryosphere*, 14:1971–1984, 6 2020. Publisher: Copernicus GmbH.

[81] Jonathan J Day and Kevin I Hodges. Growing land-sea temperature contrast and the intensification of arctic cyclones. *Geophysical Research Letters*, 45:3673–3681, 2018.

[82] M. D. Shupe. Clouds at arctic atmospheric observatories. part ii: Thermodynamic phase characteristics. *J. Appl. Meteor. Climatol.*, 50:645–661, 2011.

[83] S. Y. Matrosov Shupe, M. D. and T. Uttal. Arctic mixed-phase cloud properties derived from surface-based sensors at sheba. *J. Atmos. Sci.*, 63:697–711, 2006.

[84] Rainer Knust. Station list and links to master tracks in different resolutions of polarstern cruise ps105 (ant-xxxii/4), punta arenas - bremerhaven, 2017-03-21 - 2017-04-

20, 2017. Backup Publisher: Alfred Wegener Institute, Helmholtz Centre for Polar and Marine Research, Bremerhaven.

[85] Drift.

[86] Mosaic in numbers.

[87] Matthew D. Shupe, Markus Rex, Byron Blomquist, P. Ola G. Persson, Julia Schmale, Taneil Uttal, Dietrich Althausen, Hélène Angot, Stephen Archer, Ludovic Bariteau, Ivo Beck, John Bilberry, Silvia Bucci, Clifton Buck, Matt Boyer, Zoé Brasseur, Ian M. Brooks, Radiance Calmer, John Cassano, Vagner Castro, David Chu, David Costa, Christopher J. Cox, Jessie Creamean, Susanne Crewell, Sandro Dahlke, Ellen Damm, Gijs de Boer, Holger Deckelmann, Klaus Dethloff, Marina Dütsch, Kerstin Ebell, André Ehrlich, Jody Ellis, Ronny Engelmann, Allison A. Fong, Markus M. Frey, Michael R. Gallagher, Laurens Ganzeveld, Rolf Gradinger, Jürgen Graeser, Vernon Greenamyer, Hannes Griesche, Steele Griffiths, Jonathan Hamilton, Günther Heinemann, Detlev Helmig, Andreas Herber, Céline Heuzé, Julian Hofer, Todd Houchens, Dean Howard, Jun Inoue, Hans Werner Jacobi, Ralf Jaiser, Tuija Jokinen, Olivier Jourdan, Gina Jozef, Wessley King, Amelie Kirchgaessner, Marcus Klingebiel, Misha Krassovski, Thomas Krumpen, Astrid Lampert, William Landing, Tiia Laurila, Dale Lawrence, Michael Lonardi, Brice Loose, Christof Lüpkes, Maximilian Maahn, Andreas Macke, Wieslaw Maslowski, Christopher Marsay, Marion Maturilli, Mario Mech, Sara Morris, Manuel Moser, Marcel Nicolaus, Paul Ortega, Jackson Osborn, Falk Pätzold, Donald K. Perovich, Tuukka Petäjä, Christian Pilz, Roberta Pirazzini, Kevin Posman, Heath Powers, Kerri A. Pratt, Andreas Preußer, Lauriane Quéléver, Martin Radenz, Benjamin Rabe, Annette Rinke, Torsten Sachs, Alexander Schulz, Holger Siebert, Tercio Silva, Amy Solomon, Anja Sommerfeld, Gunnar Spreen, Mark Stephens, Andreas Stohl, Gunilla Svensson, Janek Uin, Juarez Viegas, Christiane Voigt, Peter von der Ga-

then, Birgit Wehner, Jeffrey M. Welker, Manfred Wendisch, Martin Werner, Zhou Qing Xie, and Fange Yue. Overview of the mosaic expedition- atmosphere, 2 2022.

[88] Marcel Nicolaus, Donald K Perovich, Gunnar Spreen, Mats A Granskog, Luisa von Albedyll, Michael Angelopoulos, Philipp Anhaus, Stefanie Arndt, H Jakob Belter, Vladimir Bessonov, Gerit Birnbaum, Jörg Brauchle, Radiance Calmer, Estel Cardellach, Bin Cheng, David Clemens-Sewall, Ruzica Dadic, Ellen Damm, Gijs de Boer, Oguz Demir, Klaus Dethloff, Dmitry V Divine, Allison A Fong, Steven Fons, Markus M Frey, Niels Fuchs, Carolina Gabarró, Sebastian Gerland, Helge F Goessling, Rolf Gradinger, Jari Haapala, Christian Haas, Jonathan Hamilton, Henna-Reetta Hannula, Stefan Hendricks, Andreas Herber, Céline Heuzé, Mario Hoppmann, Knut Vilhelm Høyland, Marcus Huntemann, Jennifer K Hutchings, Byongjun Hwang, Polona Itkin, Hans-Werner Jacobi, Matthias Jaggi, Arttu Jutila, Lars Kaleschke, Christian Katlein, Nikolai Kolabutin, Daniela Krampe, Steen Savstrup Kristensen, Thomas Krumpen, Nathan Kurtz, Astrid Lampert, Benjamin Allen Lange, Ruibo Lei, Bonnie Light, Felix Linhardt, Glen E Liston, Brice Loose, Amy R Macfarlane, Mallik Mahmud, Ilkka O Matero, Sönke Maus, Anne Morgenstern, Reza Naderpour, Vishnu Nandan, Alexey Niubom, Marc Oggier, Natascha Oppelt, Falk Pätzold, Christophe Perron, Tomasz Petrovsky, Roberta Pirazzini, Chris Polashenski, Benjamin Rabe, Ian A Raphael, Julia Regnery, Markus Rex, Robert Ricker, Kathrin Riemann-Campe, Annette Rinke, Jan Rohde, Evgenii Salganik, Randall K Scharien, Martin Schiller, Martin Schneebeli, Maximilian Semmling, Egor Shimanchuk, Matthew D Shupe, Madison M Smith, Vasily Smolyanitsky, Vladimir Sokolov, Tim Stanton, Julienne Stroeve, Linda Thielke, Anna Timofeeva, Rasmus Tage Tonboe, Aikaterini Tavri, Michel Tsamados, David N Wagner, Daniel Watkins, Melinda Webster, and Manfred Wendisch. Overview of the mosaic expedition: Snow and sea ice. *Elementa: Science of the Anthropocene*, 10:000046, 2 2022.

[89] Benjamin Rabe, Céline Heuzé, Julia Regnery, Yevgeny Aksenov, Jacob Allerholt, Marylou Athanase, Youcheng Bai, Chris Basque, Dorothea Bauch, Till M Baumann, Dake Chen, Sylvia T Cole, Lisa Craw, Andrew Davies, Ellen Damm, Klaus Dethloff, Dmitry V Divine, Francesca Doglioni, Falk Ebert, Ying-Chih Fang, Ilker Fer, Allison A Fong, Rolf Gradinger, Mats A Granskog, Rainer Graupner, Christian Haas, Hailun He, Yan He, Mario Hoppmann, Markus Janout, David Kadko, Torsten Kanzow, Salar Karam, Yusuke Kawaguchi, Zoe Koenig, Bin Kong, Richard A Krishfield, Thomas Krumpen, David Kuhlmey, Ivan Kuznetsov, Musheng Lan, Georgi Laukert, Ruibo Lei, Tao Li, Sinhué Torres-Valdés, Lina Lin, Long Lin, Hailong Liu, Na Liu, Brice Loose, Xiaobing Ma, Rosalie McKay, Maria Mallet, Robbie D C Mallett, Wieslaw Maslowski, Christian Mertens, Volker Mohrholz, Morven Muilwijk, Marcel Nicolaus, Jeffrey K O'Brien, Donald Perovich, Jian Ren, Markus Rex, Natalia Ribeiro, Annette Rinke, Janin Schaffer, Ingo Schuffenhauer, Kirstin Schulz, Matthew D Shupe, William Shaw, Vladimir Sokolov, Anja Sommerfeld, Gunnar Spreen, Timothy Stanton, Mark Stephens, Jie Su, Natalia Sukhikh, Arild Sundfjord, Karolin Thomisch, Sandra Tippenhauer, John M Toole, Myriel Vredenborg, Maren Walter, Hangzhou Wang, Lei Wang, Yuntao Wang, Manfred Wendisch, Jinping Zhao, Meng Zhou, and Jialiang Zhu. Overview of the mosaic expedition: Physical oceanography. *Elementa: Science of the Anthropocene*, 10:00062, 2 2022.

[90] Allison A Fong, Clara J M Hoppe, Nicole Aberle, Carin J Ashjian, Philipp Assmy, Youcheng Bai, Dorothee C E Bakker, John P Balmonte, Kevin R Barry, Stefan Bertilsson, William Boulton, Jeff Bowman, Deborah Bozzato, Gunnar Bratbak, Moritz Buck, Robert G Campbell, Giulia Castellani, Emelia J Chamberlain, Jianfang Chen, Melissa Chierici, Astrid Cornils, Jessie M Creamean, Ellen Damm, Klaus Dethloff, Elise S Droste, Oliver Ebenhöh, Sarah L Eggers, Anja Engel, Hauke Flores, Agneta Fransson, Stephan Frickenhaus, Jessie Gardner, Cecilia E Gelfman, Mats A Granskog, Martin Graeve, Charlotte Havermans, Céline Heuzé, Nicole Hildebrandt, Thomas C J

Hill, Mario Hoppema, Antonia Immerz, Haiyan Jin, Boris P Koch, Xianyu Kong, Alexandra Kraberg, Musheng Lan, Benjamin A Lange, Aud Larsen, Benoit Lebreton, Eva Leu, Brice Loose, Wieslaw Maslowski, Camille Mavis, Katja Metfies, Thomas Mock, Oliver Müller, Marcel Nicolaus, Barbara Niehoff, Daiki Nomura, Eva-Maria Nöthig, Marc Oggier, Ellen Oldenburg, Lasse Mork Olsen, Ilka Peeken, Donald K Perovich, Ovidiu Popa, Benjamin Rabe, Jian Ren, Markus Rex, Annette Rinke, Sebastian Rokitta, Björn Rost, Serdar Sakinan, Evgenii Salganik, Fokje L Schaafsma, Hendrik Schäfer, Katrin Schmidt, Katyanne M Shoemaker, Matthew D Shupe, Pauline Snoeijs-Leijonmalm, Jacqueline Stefels, Anders Svenson, Ran Tao, Sinhué Torres-Valdés, Anders Torstensson, Andrew Toseland, Adam Ulfsbo, Maria A Van Leeuwe, Martina Vortkamp, Alison L Webb, Yanpei Zhuang, and Rolf R Gradinger. Overview of the mosaic expedition: Ecosystem. *Elementa: Science of the Anthropocene*, 12:135, 8 2024.

[91] Hannah C Frostenberg, André Welti, Mikael Luhr, Julien Savre, Erik S Thomson, and Luisa Ickes. The chance of freezing – a conceptional study to parameterize temperature-dependent freezing by including randomness of ice-nucleating particle concentrations. *Atmospheric Chemistry and Physics*, 23:10883–10900, 10 2023. Publisher: Copernicus GmbH.

[92] Jessie M Creamean, Katherine M Primm, Margaret A Tolbert, Emrys G Hall, Jim Wendell, Allen Jordan, Patrick J Sheridan, Jedediah Smith, and Russell C Schnell. Hovercat: a novel aerial system for evaluation of aerosol–cloud interactions. *Atmospheric Measurement Techniques*, 11:3969–3985, 7 2018. Publisher: Copernicus GmbH.

[93] Jesse Creamean, Thomas Hill, Carson Hume, and Timothy Devadoss. Ice nucleation spectrometer (ins) instrument handbook, 3 2024.

[94] Gabor Vali. Quantitative evaluation of experimental results an the heterogeneous freezing nucleation of supercooled liquids. *Journal of Atmospheric Sciences*, 28:402 – 409, 1971.

[95] Annette Rinke, John Cassano, Elizabeth Cassano, Ralf Jaiser, and Dörthe Handorf. Meteorological conditions during the mosaic expedition. *Elementa: Science of the Anthropocene*, 9, 9 2021.

[96] Alan Agresti and Brent A. Coull. Approximate is better than "exact" for interval estimation of binomial proportions. *American Statistician*, 52:119–126, 1998.

[97] Tom C J Hill, Paul J DeMott, Yutaka Tobo, Janine Fröhlich-Nowoisky, Bruce F Moffett, Gary D Franc, and Sonia M Kreidenweis. Sources of organic ice nucleating particles in soils. *Atmospheric Chemistry and Physics*, 16:7195–7211, 6 2016. Publisher: Copernicus GmbH.

[98] Kaitlyn J Suski, Tom C J Hill, Ezra J T Levin, Anna Miller, Paul J DeMott, and Sonia M Kreidenweis. Agricultural harvesting emissions of ice-nucleating particles. *Atmospheric Chemistry and Physics*, 18:13755–13771, 9 2018. Publisher: Copernicus GmbH.

[99] Christina S McCluskey, Jurgita Ovadnevaite, Matteo Rinaldi, James Atkinson, Franco Belosi, Darius Ceburnis, Salvatore Marullo, Thomas C J Hill, Ulrike Lohmann, Zamin A Kanji, Colin O'Dowd, Sonia M Kreidenweis, and Paul J DeMott. Marine and terrestrial organic ice-nucleating particles in pristine marine to continentally influenced northeast atlantic air masses. *Journal of Geophysical Research: Atmospheres*, 123:6196–6212, 2018.

[100] N P Fofonoff and R C Millard Jr. Algorithms for the computation of fundamental properties of seawater. 1983. Accepted: 2014-02-14T11:16:56Z Publisher: UNESCO.

[101] Christopher Cox, Michael Gallagher, Matthew Shupe, Ola Persson, Byron Blomquist, Andrey Grachev, Laura Riihimaki, Mark Kutchenreiter, Victor Morris, Amy Solomon, Ian Brooks, David Costa, Daniel Gottas, Jennifer Hutchings, Jackson Osborn, Sara Morris, Andreas Preusser, and Taneil Uttal. Met city meteorological and surface flux

measurements (level 2 processed), multidisciplinary drifting observatory for the study of arctic climate (mosaic), central arctic, october 2019 - september 2020. 2023. Publisher: urn:node:ARCTIC.

[102] John D Hunter. Matplotlib: A 2d graphics environment. *Computing in Science Engineering*, 9:90–95, 5 2007. Conference Name: Computing in Science Engineering.

[103] Charles R Harris, K Jarrod Millman, Stéfan J van der Walt, Ralf Gommers, Pauli Virtanen, David Cournapeau, Eric Wieser, Julian Taylor, Sebastian Berg, Nathaniel J Smith, Robert Kern, Matti Picus, Stephan Hoyer, Marten H van Kerkwijk, Matthew Brett, Allan Haldane, Jaime Fernández del Río, Mark Wiebe, Pearu Peterson, Pierre Gérard-Marchant, Kevin Sheppard, Tyler Reddy, Warren Weckesser, Hameer Abbasi, Christoph Gohlke, and Travis E Oliphant. Array programming with numpy. *Nature*, 585:357–362, 9 2020. Publisher: Nature Publishing Group.

[104] Ivo Beck, Hélène Angot, Andrea Baccarini, Lubna Dada, Lauriane Quéléver, Tuija Jokinen, Tiia Laurila, Markus Lampimäki, Nicolas Bukowiecki, Matthew Boyer, Xianda Gong, Martin Gysel-Beer, Tuukka Petäjä, Jian Wang, and Julia Schmale. Automated identification of local contamination in remote atmospheric composition time series. *Atmospheric Measurement Techniques*, 15:4195–4224, 7 2022. Publisher: Copernicus GmbH.

[105] Nora Bergner, Ivo Beck, Lauriane Quéléver, Tuija Jokinen, Tiia Laurila, Lubna Dada, and Julia Schmale. Aerodynamic particle sizer spectrometer (aps) aerosol number concentrations, measured in the swiss container during mosaic 2019/2020, 2023.

[106] Ivo Beck, Lauriane Quéléver, Tiia Laurila, Tuija Jokinen, and Julia Schmale. Continuous corrected particle number concentration data in 10 sec resolution measured in the swiss aerosol container using a whole air inlet during mosaic 2019/2020, 2023.

[107] Flexpart simulations for mosaic.

[108] Stewart J. S. Meier W. N Fetterer, F. Masam2: Daily 4 km arctic sea ice concentration. (g10005, version 2). [data set]. *National Snow and Ice Data Center*, 2023.

[109] Jiawei Zhuang, raphael dussin, David Huard, Pascal Bourgault, Anderson Banihirwe, Stephane Raynaud, Brewster Malevich, Martin Schupfner, Filipe, Sam Levang, Charles Gauthier, André Jüling, Mattia Almansi, RichardScottOZ, RondeauG, Stephan Rasp, Trevor James Smith, Jemma Stachelek, Matthew Plough, Pierre, Ray Bell, Romain Caneill, and Xianxiang Li. pangeo-data/xesmf: v0.8.2, 9 2023.

[110] T J Ballinger, J E Overland, M Wang, U S Bhatt, E Hanna, I Hanssen-Bauer, S.-J. Kim, R L Thoman, and J E Walsh. Arctic report card 2020: Surface air temperature.

[111] M. D. Shupe I. M. Brooks P. Achtert J. Prytherch Tjernström, M. and J. Sedlar. Arctic summer airmass transformation, surface inversions, and the surface energy budget. *J. Climate*, 32:769–789, 2019.

[112] Cassano J. J. Dahlke S. Dice M. Cox C. J. Jozef, G. C. and G. de Boer. An overview of the vertical structure of the atmospheric boundary layer in the central arctic during mosaic. *Atmos. Chem. Phys.*, 24:1429–1450, 2024.

[113] Melinda A Webster, Marika Holland, Nicholas C Wright, Stefan Hendricks, Nils Hutter, Polona Itkin, Bonnie Light, Felix Linhardt, Donald K Perovich, Ian A Raphael, Madison M Smith, Luisa von Albedyll, and Jinlun Zhang. Spatiotemporal evolution of melt ponds on arctic sea ice: Mosaic observations and model results. *Elementa: Science of the Anthropocene*, 10:000072, 5 2022.

[114] Linette N Boisvert, Melinda A Webster, Chelsea L Parker, and Richard M Forbes. Rainy days in the arctic. *Journal of Climate*, 36:6855–6878, 9 2023. Publisher: American Meteorological Society Section: Journal of Climate.

[115] R Bintanja and O Andry. Towards a rain-dominated arctic. *Nature Climate Change*, 7:263–267, 4 2017. Publisher: Nature Publishing Group.

[116] Thomas Stocker. *Climate Change 2013: The Physical Science Basis: Working Group I Contribution to the Fifth Assessment Report of the Intergovernmental Panel on Climate Change*. Cambridge University Press, 3 2014. Google-Books-ID: o4gaBQAAQBAJ.

[117] E B Łupikasza and K Cielecka-Nowak. Changing probabilities of days with snow and rain in the atlantic sector of the arctic under the current warming trend. *Journal of Climate*, 33:2509–2532, 3 2020. Publisher: American Meteorological Society Section: Journal of Climate.

[118] Persson O. Shupe M. Solomon A. Gallagher M. Lawrence Z. Perovich D. Cox, C. Driving mechanisms for the onset of the summer melt season at mosaic. *AGU Fall Meeting Abstracts*, 2021.

[119] Nicholas Wright, Melinda Webster, and Chris Polashenski. Melt pond maps around the multidisciplinary drifting observatory for the study of arctic climate (mosaic) drifting station derived from high resolution optical imagery, 2020. 2021. Publisher: urn:node:ARCTIC.

[120] Melinda A Webster, Ignatius G Rigor, Donald K Perovich, Jacqueline A Richter-Menge, Christopher M Polashenski, and Bonnie Light. Seasonal evolution of melt ponds on arctic sea ice. *Journal of Geophysical Research: Oceans*, 120:5968–5982, 2015.

[121] Polona Itkin, Stefan Hendricks, Melinda Webster, Luisa von Albedyll, Stefanie Arndt, Dmitry Divine, Matthias Jaggi, Marc Oggier, Ian Raphael, Robert Ricker, Jan Rohde, Martin Schneebeli, and Glen E Liston. Sea ice and snow characteristics from year-long transects at the mosaic central observatory. *Elementa: Science of the Anthropocene*, 11:48, 2 2023.

[122] Ian A Raphael, Donald K Perovich, Christopher M Polashenski, David Clemens-Sewall, Polona Itkin, Ruibo Lei, Marcel Nicolaus, Julia Regnery, Madison M Smith, Melinda Webster, and Matthias Jaggi. Sea ice mass balance during the mosaic drift experiment: Results from manual ice and snow thickness gauges. *Elementa: Science of the Anthropocene*, 12:00040, 7 2024.

[123] Hannah Niehaus, Larysa Istomina, Marcel Nicolaus, Ran Tao, Aleksey Malinka, Eleonora Zege, and Gunnar Spreen. Melt pond fractions on arctic summer sea ice retrieved from sentinel-3 satellite data with a constrained physical forward model. *The Cryosphere*, 18:933–956, 2 2024.

[124] Aliaga-D. Pernov J. B. Angot H. Quéléver L. L. J. Dada L. Heutte B. Dall'Osto-M. Beddows D. C. S. Brasseur Z. Beck I. Bucci S. Duetsch M. Stohl A. Laurila T. Asmi E. Massling A. Thomas D. C. Nøjgaard J. K. Chan T. Sharma S. Tunved P. Krejci R. Hansson H. C. Bianchi F. Lehtipalo K. Wiedensohler A. Weinhold K. Kulmala M. Petäjä T. Sipilä M. Schmale J. Boyer, M. and T. Jokinen. A full year of aerosol size distribution data from the central arctic under an extreme positive arctic oscillation: insights from the multidisciplinary drifting observatory for the study of arctic climate (mosaic) expedition. *Atmos. Chem. Phys.*, 23:389–415, 2023.

[125] Gabor Vali. Sizes of atmospheric ice nuclei. *Nature*, 212:384–385, 10 1966. Publisher: Nature Publishing Group.

[126] E Keith Bigg, Caroline Leck, and Lars Tranvik. Particulates of the surface microlayer of open water in the central arctic ocean in summer. *Marine Chemistry*, 91:131–141, 11 2004.

[127] Ladino-L. Alpert P. et al. Wilson, T. A marine biogenic source of atmospheric ice-nucleating particles. *Nature*, 525:234–238, 2015.

[128] R H Mason, M Si, C Chou, V E Irish, R Dickie, P Elizondo, R Wong, M Brintnell, M Elsasser, W M Lassar, K M Pierce, W R Leaitch, A M MacDonald, A Platt, D Toom-Sauntry, R Sarda-Estève, C L Schiller, K J Suski, T C J Hill, J P D Abbatt, J A Huffman, P J DeMott, and A K Bertram. Size-resolved measurements of ice-nucleating particles at six locations in north america and one in europe. *Atmospheric Chemistry and Physics*, 16:1637–1651, 2 2016. Publisher: Copernicus GmbH.

[129] Christina S McCluskey, Thomas C J Hill, Camille M Sultana, Olga Laskina, Jonathan Trueblood, Mitchell V Santander, Charlotte M Beall, Jennifer M Michaud, Sonia M Kreidenweis, Kimberly A Prather, Vicki Grassian, and Paul J DeMott. A mesocosm double feature: Insights into the chemical makeup of marine ice nucleating particles. *Journal of the Atmospheric Sciences*, 75:2405 – 2423, 2018.

[130] D A Knopf, P A Alpert, B Wang, and J Y Aller. Stimulation of ice nucleation by marine diatoms. *Nature Geoscience*, 4:88–90, 2 2011. Publisher: Nature Publishing Group.

[131] R C Schnell and G Vali. Freezing nuclei in marine waters. *Tellus A: Dynamic Meteorology and Oceanography*, 27, 1 1975.

[132] Ivo Beck, Alireza Moallemi, Benjamin Heutte, Jakob Boyd Pernov, Nora Bergner, Margarida Rolo, Lauriane L J Quéléver, Tiia Laurila, Matthew Boyer, Tuija Jokinen, Hélène Angot, Clara J M Hoppe, Oliver Müller, Jessie Creamean, Markus M Frey, Gabriel Freitas, Julika Zinke, Matt Salter, Paul Zieger, Jessica A Mirrielees, Hailey E Kempf, Andrew P Ault, Kerri A Pratt, Martin Gysel-Beer, Silvia Henning, Christian Tatzelt, and Julia Schmale. Characteristics and sources of fluorescent aerosols in the central arctic ocean. *Elementa: Science of the Anthropocene*, 12:125, 5 2024.

[133] Nicole J Savage, Christine E Krentz, Tobias Könemann, Taewon T Han, Gediminas Mainelis, Christopher Pöhlker, and J Alex Huffman. Systematic characterization and

fluorescence threshold strategies for the wideband integrated bioaerosol sensor (wibs) using size-resolved biological and interfering particles. *Atmospheric Measurement Techniques*, 10:4279–4302, 11 2017. Publisher: Copernicus GmbH.

[134] Alireza Moallemi, Sebastian Landwehr, Charlotte Robinson, Rafel Simó, Marina Zamanillo, Gang Chen, Andrea Baccarini, Martin Schnaiter, Silvia Henning, Robin L Modini, Martin Gysel-Beer, and Julia Schmale. Sources, occurrence and characteristics of fluorescent biological aerosol particles measured over the pristine southern ocean. *Journal of Geophysical Research: Atmospheres*, 126:e2021JD034811, 2021.

[135] A E Perring, J P Schwarz, D Baumgardner, M T Hernandez, D V Spracklen, C L Heald, R S Gao, G Kok, G R McMeeking, J B McQuaid, and D W Fahey. Airborne observations of regional variation in fluorescent aerosol across the united states. *Journal of Geophysical Research: Atmospheres*, 120:1153–1170, 2015.

[136] Carlos del Blanco Alegre, Amaya Castro, Ana Calvo, Fernanda Oduber, Elisabeth Alonso-Blanco, Delia Fernandez Gonzalez, Rosa M Valencia-Barrera, Ana Vega-Maray, and Roberto Fraile. Below-cloud scavenging of fine and coarse aerosol particles by rain: The role of raindrop size. *Quarterly Journal of the Royal Meteorological Society*, 144, 9 2018.

[137] Kimberly A Prather, Timothy H Bertram, Vicki H Grassian, Grant B Deane, M Dale Stokes, Paul J DeMott, Lihini I Aluwihare, Brian P Palenik, Farooq Azam, John H Seinfeld, Ryan C Moffet, Mario J Molina, Christopher D Cappa, Franz M Geiger, Gregory C Roberts, Lynn M Russell, Andrew P Ault, Jonas Baltrusaitis, Douglas B Collins, Craig E Corrigan, Luis A Cuadra-Rodriguez, Carlena J Ebben, Sara D Forestieri, Timothy L Guasco, Scott P Hersey, Michelle J Kim, William F Lambert, Robin L Modini, Wilton Mui, Byron E Pedler, Matthew J Ruppel, Olivia S Ryder, Nathan G Schoepp, Ryan C Sullivan, and Defeng Zhao. Bringing the ocean into the laboratory to probe the chemical complexity of sea spray aerosol. *Proceedings of the*

National Academy of Sciences, 110:7550–7555, 5 2013. Publisher: Proceedings of the National Academy of Sciences.

[138] Congbo Song, Manuel Dall'Osto, Angelo Lupi, Mauro Mazzola, Rita Traversi, Silvia Becagli, Stefania Gilardoni, Stergios Vratolis, Karl Espen Yttri, David C S Beddows, Julia Schmale, James Brean, Agung Ghani Kramawijaya, Roy M Harrison, and Zongbo Shi. Differentiation of coarse-mode anthropogenic, marine and dust particles in the high arctic islands of svalbard. *Atmospheric Chemistry and Physics*, 21:11317–11335, 7 2021. Publisher: Copernicus GmbH.

[139] C Hoose and O Möhler. Heterogeneous ice nucleation on atmospheric aerosols: a review of results from laboratory experiments. *Atmospheric Chemistry and Physics*, 12:9817–9854, 2012.

[140] Bettina Weber J. Alex Huffman Christopher Pöhlker Meinrat O. Andreae Naama Lang-Yona Susannah M. Burrows Sachin S. Gunthe Wolfgang Elbert Hang Su Peter Hoor Eckhard Thines Thorsten Hoffmann Viviane R. Després Ulrich Pöschl Janine Fröhlich-Nowoisky, Christopher J. Kampf. Bioaerosols in the earth system: Climate, health, and ecosystem interactions. *Atmospheric Research*, 182:346–376, 2016.

[141] Zamin A Kanji, Luis A Ladino, Heike Wex, Yvonne Boose, Monika Burkert-Kohn, Daniel J Cziczo, and Martina Krämer. Overview of ice nucleating particles. *Meteorological Monographs*, 58:1.1–1.33, 1 2017. Publisher: American Meteorological Society Section: Meteorological Monographs.

[142] Shu Huang, Wei Hu, Jie Chen, Zhijun Wu, Daizhou Zhang, and Pingqing Fu. Overview of biological ice nucleating particles in the atmosphere. *Environment International*, 146:106197, 1 2021.

[143] M Joly, P Amato, L Deguillaume, M Monier, C Hoose, and A.-M. Delort. Quantification of ice nuclei active at near 0 °c temperatures in low-altitude clouds at the puy

de dôme atmospheric station. *Atmospheric Chemistry and Physics*, 14:8185–8195, 8 2014. Publisher: Copernicus GmbH.

[144] D J Bowles, P J Lillford, D A Rees, I A Shanks, and Rolv Lundheim. Physiological and ecological significance of biological ice nucleators. *Philosophical Transactions of the Royal Society of London. Series B: Biological Sciences*, 357:937–943, 7 2002. Publisher: Royal Society.

[145] B J Murray, D O'Sullivan, J D Atkinson, and M E Webb. Ice nucleation by particles immersed in supercooled cloud droplets. *Chemical Society Reviews*, 41:6519, 2012.

[146] P A Alpert, J Y Aller, and D A Knopf. Ice nucleation from aqueous nacl droplets with and without marine diatoms. *Atmospheric Chemistry and Physics*, 11:5539–5555, 6 2011. Publisher: Copernicus GmbH.

[147] Susannah M Burrows Corinna Hoose AleksandrS. Safatov Galina Buryak Janine Fröhlich-Nowoisky Wolfgang Elbert MeinratO. Andreae Ulrich Pöschl VivianeR. Després J.Alex Huffman and Ruprecht Jaenicke. Primary biological aerosol particles in the atmosphere: a review. *Tellus B: Chemical and Physical Meteorology*, 64:15598, 2012.

[148] Markus Hartmann Astrid Bracher Frank Stratmann-Hartmut Herrmann Sebastian Zeppenfeld, Manuela van Pinxteren. Glucose as a potential chemical marker for ice nucleating activity in arctic seawater and melt pond samples. *Environmental Science Technology*, 2019.

[149] Dapeng Xu, Hejun Kong, Eun-Jin Yang, Xinran Li, Nianzhi Jiao, Alan Warren, Ying Wang, Youngju Lee, Jinyoung Jung, and Sung-Ho Kang. Contrasting community composition of active microbial eukaryotes in melt ponds and sea water of the arctic ocean revealed by high throughput sequencing. *Frontiers in Microbiology*, 11, 6 2020. Publisher: Frontiers.

[150] S M Burrows, C Hoose, U Pöschl, and M G Lawrence. Ice nuclei in marine air: biogenic particles or dust? *Atmospheric Chemistry and Physics*, 13:245–267, 1 2013. Publisher: Copernicus GmbH.

[151] R C Schnell and Gabor Vali. Biogenic ice nuclei: Part i. terrestrial and marine sources. *Journal of the Atmospheric Sciences*, 33:1554–1564, 8 1976. Publisher: American Meteorological Society Section: Journal of the Atmospheric Sciences.

[152] Philipp Assmy, Jens K Ehn, Mar Fernández-Méndez, Haakon Hop, Christian Katlein, Arild Sundfjord, Katrin Bluhm, Malin Daase, Anja Engel, Agneta Fransson, Mats A Granskog, Stephen R Hudson, Svein Kristiansen, Marcel Nicolaus, Ilka Peeken, Angelika H H Renner, Gunnar Spreen, Agnieszka Tatarek, and Jozef Wiktor. Floating ice-algal aggregates below melting arctic sea ice. *PLOS ONE*, 8:e76599, 10 2013. Publisher: Public Library of Science.

[153] W S Grant and Rita A Horner. Growth responses to salinity variation in four arctic ice diatoms. *Journal of Phycology*, 12:180–185, 1976.

[154] K M Lewis, A E Arntsen, P Coupel, H Joy-Warren, K E Lowry, A Matsuoka, M M Mills, G L van Dijken, V Selz, and K R Arrigo. Photoacclimation of arctic ocean phytoplankton to shifting light and nutrient limitation. *Limnology and Oceanography*, 64:284–301, 2019.

[155] C J Mundy, Michel Gosselin, Jens K Ehn, Claude Belzile, Michel Poulin, Eva Alou, Suzanne Roy, Haakon Hop, Sylvie Lessard, Tim N Papakyriakou, David G Barber, and Jeremy Stewart. Characteristics of two distinct high-light acclimated algal communities during advanced stages of sea ice melt. *Polar Biology*, 34:1869–1886, 12 2011.

[156] Don Perovich, Madison Smith, Bonnie Light, and Melinda Webster. Meltwater sources and sinks for multiyear arctic sea ice in summer. *The Cryosphere*, 15:4517–4525, 9 2021. Publisher: Copernicus GmbH.

[157] Annette K Møller, Ditte A Søborg, Waleed Abu Al-Soud, Søren J Sørensen, and Niels Kroer. Bacterial community structure in high-arctic snow and freshwater as revealed by pyrosequencing of 16s rrna genes and cultivation. *Polar Research*, 4 2013.

[158] Ido Hatam, Benjamin Lange, Justin Beckers, Christian Haas, and Brian Lanoil. Bacterial communities from arctic seasonal sea ice are more compositionally variable than those from multi-year sea ice. *The ISME Journal*, 10:2543–2552, 10 2016.

[159] Daiki Nomura, Yusuke Kawaguchi, Alison L Webb, Yuhong Li, Manuel Dall'osto, Katrin Schmidt, Elise S Droste, Emelia J Chamberlain, Nikolai Kolabutin, Egor Shimanchuk, Mario Hoppmann, Michael R Gallagher, Hanno Meyer, Moein Mellat, Dorothea Bauch, Carolina Gabarró, Madison M Smith, Jun Inoue, Ellen Damm, and Bruno Delille. Meltwater layer dynamics in a central arctic lead: Effects of lead width, re-freezing, and mixing during late summer. *Elementa: Science of the Anthropocene*, 11:102, 5 2023.

[160] Camilla Fahlgren, Laura Gómez-Consarnau, Julia Zábori, Markus V Lindh, Radovan Krejci, E Monica Mårtensson, Douglas Nilsson, and Jarone Pinhassi. Seawater mesocosm experiments in the arctic uncover differential transfer of marine bacteria to aerosols. *Environmental Microbiology Reports*, 7:460–470, 6 2015.

[161] Josephine Z Rapp, Mar Fernández-Méndez, Christina Bienhold, and Antje Boetius. Effects of ice-algal aggregate export on the connectivity of bacterial communities in the central arctic ocean. *Frontiers in Microbiology*, 9, 5 2018. Publisher: Frontiers.

[162] T Krumpen, F Birrien, F Kauker, T Rackow, L von Albedyll, M Angelopoulos, H J Belter, V Bessonov, E Damm, K Dethloff, J Haapala, C Haas, C Harris, S Hendricks, J Hoelemann, M Hoppmann, L Kaleschke, M Karcher, N Kolabutin, R Lei, J Lenz, A Morgenstern, M Nicolaus, U Nixdorf, T Petrovsky, B Rabe, L Rabenstein, M Rex, R Ricker, J Rohde, E Shimanchuk, S Singha, V Smolyanitsky, V Sokolov, T Stanton,

A Timofeeva, M Tsamados, and D Watkins. The mosaic ice floe: sediment-laden survivor from the siberian shelf. *The Cryosphere*, 14:2173–2187, 7 2020.

[163] N W May, P K Quinn, S M McNamara, and K A Pratt. Multiyear study of the dependence of sea salt aerosol on wind speed and sea ice conditions in the coastal arctic. *Journal of Geophysical Research: Atmospheres*, 121:9208–9219, 2016.

[164] M. Norman E. K. Bigg Leck, C. and R. Hillamo. Chemical composition and sources of the high arctic aerosol relevant for cloud formation. *Journal of Geophysical Research: Atmospheres*, 2002.

[165] Asmi E. Atanasova N. S. Heikkinen A. E. Vidal-E. Duplissy J. Romantschuk M. Kouznetsov R. Kukkonen J. Bamford D. H. Hyvärinen A.-P. Sofieva, S. and M. Sofiev. Effects of temperature and salinity on bubble-bursting aerosol formation simulated with a bubble-generating chamber. *Atmos. Meas. Tech.*, 2022.

[166] Charbel Harb and Hosein Foroutan. Experimental development of a lake spray source function and its model implementation for great lakes surface emissions. *Atmospheric Chemistry and Physics*, 22:11759–11779, 9 2022. Publisher: Copernicus GmbH.

[167] Jessica L Axson, Nathaniel W May, Isabel D Colón-Bernal, Kerri A Pratt, and Andrew P Ault. Lake spray aerosol: A chemical signature from individual ambient particles. *Environmental Science Technology*, 50:9835–9845, 9 2016. Publisher: American Chemical Society.

[168] Padmanav Pallavi, D Parthasarathy, K Narayanan, A B Inamdar, and Sachin Budakoti. Examining the principal factors that limits the chlorophyll-a concentration across coastal waters of northern maharashtra state using a robust generalised additive model. *Regional Studies in Marine Science*, 77:103693, 12 2024.

[169] Markus M Frey, Sarah J Norris, Ian M Brooks, Philip S Anderson, Kouichi Nishimura, Xin Yang, Anna E Jones, Michelle G Nerentorp Mastromonaco, David H Jones, and

Eric W Wolff. First direct observation of sea salt aerosol production from blowing snow above sea ice. *Atmospheric Chemistry and Physics*, 20:2549–2578, 3 2020. Publisher: Copernicus GmbH.

[170] Xianda Gong, Jiaoshi Zhang, Betty Croft, Xin Yang, Markus M Frey, Nora Bergner, Rachel Y.-W. Chang, Jessie M Creamean, Chongai Kuang, Randall V Martin, Ananth Ranjithkumar, Arthur J Sedlacek, Janek Uin, Sascha Willmes, Maria A Zawadowicz, Jeffrey R Pierce, Matthew D Shupe, Julia Schmale, and Jian Wang. Arctic warming by abundant fine sea salt aerosols from blowing snow. *Nature Geoscience*, 16:768–774, 9 2023. Publisher: Nature Publishing Group.

[171] Jiayue Huang and Lyatt Jaeglé. Wintertime enhancements of sea salt aerosol in polar regions consistent with a sea ice source from blowing snow. *Atmospheric Chemistry and Physics*, 17:3699–3712, 3 2017. Publisher: Copernicus GmbH.

[172] Ernie R Lewis and Stephen E Schwartz. *Sea Salt Aerosol Production Fluxes: Estimates and Critical Analysis*, pages 299–344. American Geophysical Union (AGU), 2004.

[173] Michael Lonardi, Christian Pilz, Elisa F Akansu, Sandro Dahlke, Ulrike Egerer, André Ehrlich, Hannes Griesche, Andrew J Heymsfield, Benjamin Kirbus, Carl G Schmitt, Matthew D Shupe, Holger Siebert, Birgit Wehner, and Manfred Wendisch. Tethered balloon-borne profile measurements of atmospheric properties in the cloudy atmospheric boundary layer over the arctic sea ice during mosaic: Overview and first results. *Elementa: Science of the Anthropocene*, 10:000120, 9 2022.

[174] H J Griesche, K Ohneiser, P Seifert, M Radenz, R Engelmann, and A Ansmann. Contrasting ice formation in arctic clouds: surface-coupled vs. surface-decoupled clouds. *Atmos. Chem. Phys.*, 21:10357–10374, 7 2021.

[175] Anca Gaman, Üllar Rannik, Pasi Aalto, Toivo Pohja, Erkki Siivola, Markku Kulmala, and Timo Vesala. Relaxed eddy accumulation system for size-resolved aerosol particle

flux measurements. *Journal of Atmospheric and Oceanic Technology*, 21:933–943, 6 2004. Publisher: American Meteorological Society Section: Journal of Atmospheric and Oceanic Technology.

[176] Victor Morris, Brian Ermold, Damao Zhang, and Yan Shi. Boundary-layer height data with ceil (ceilpblht).

[177] Sandro Dahlke, Matthew D Shupe, Christopher J Cox, Ian M Brooks, Byron Blomquist, and P Ola G Persson. Extended radiosonde profiles 2019/09-2020/10 during mosaic legs ps122/1 - ps122/5, 2023.

[178] David Bolton. The computation of equivalent potential temperature. *Monthly Weather Review*, 108:1046–1053, 7 1980. Publisher: American Meteorological Society Section: Monthly Weather Review.

Appendix A

Supporting Information

A.1 Supplemental Figures

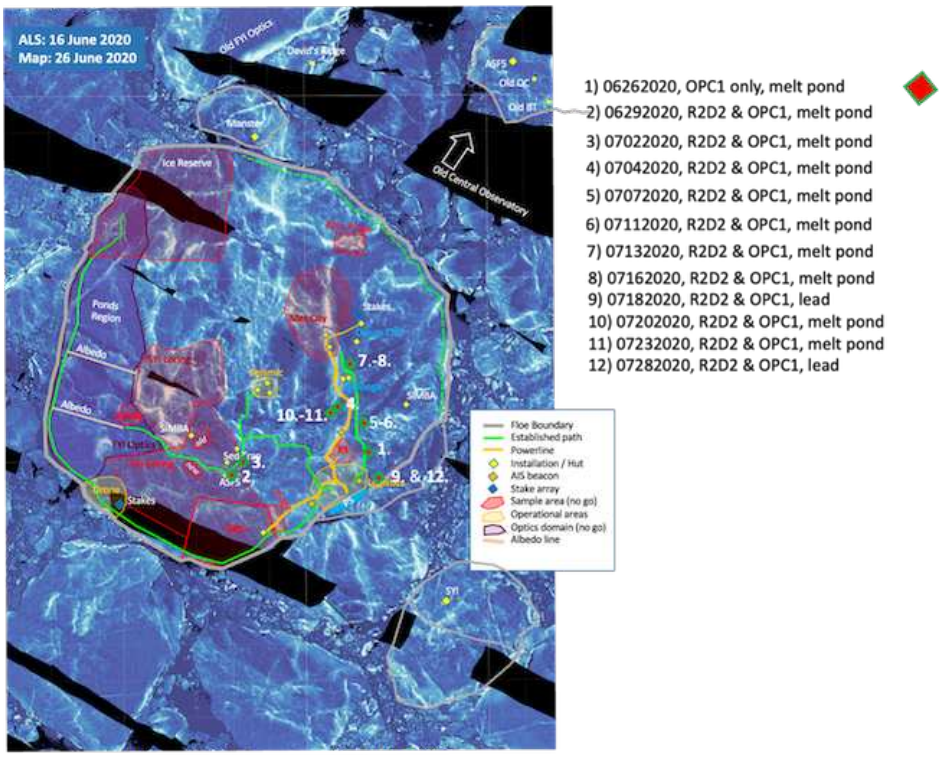

Figure A.1: Map of the MOSAiC Central Observatory based on ALS scans from the helicopter during July 2020 in which the location of each ice station (numbered) with respect to *Polarstern* (blue rectangle, bottom-right of floe boundary) is marked with a red-diamond. Image credit: Matthew Shupe, Tuija Jokinen.

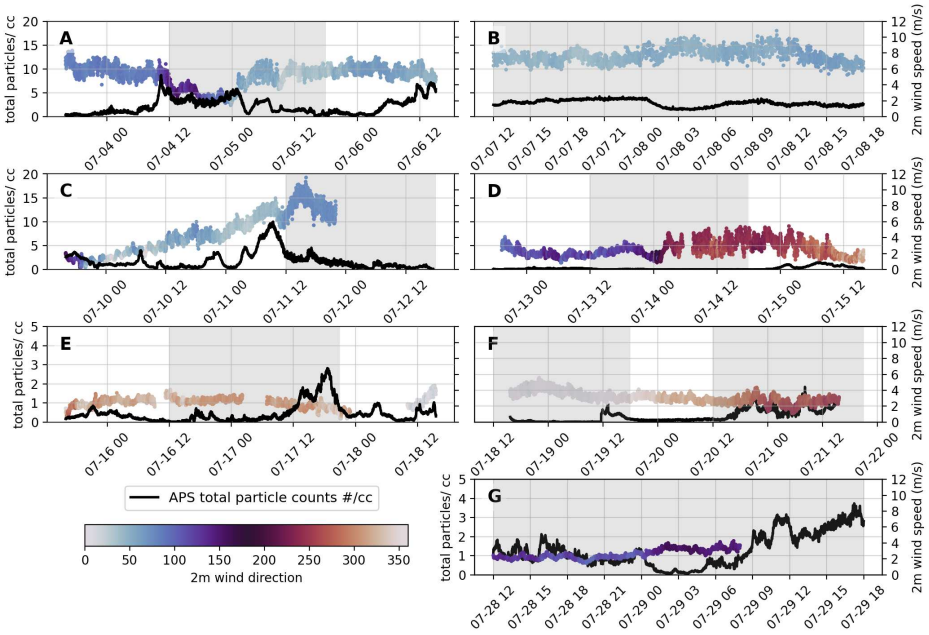

Figure A.2: 1-min averaged supermicron total particle counts (black line) and 2 m wind speeds (dots colored by 2 m wind direction). The x-axes of panels A, C, D, E, F span the on-board filter sampling period (3 days) where the gray shading defines the on-ice sampling periods (No on-board filters for B and G). Note the scales of the left y-axis differ for the bottom two rows.

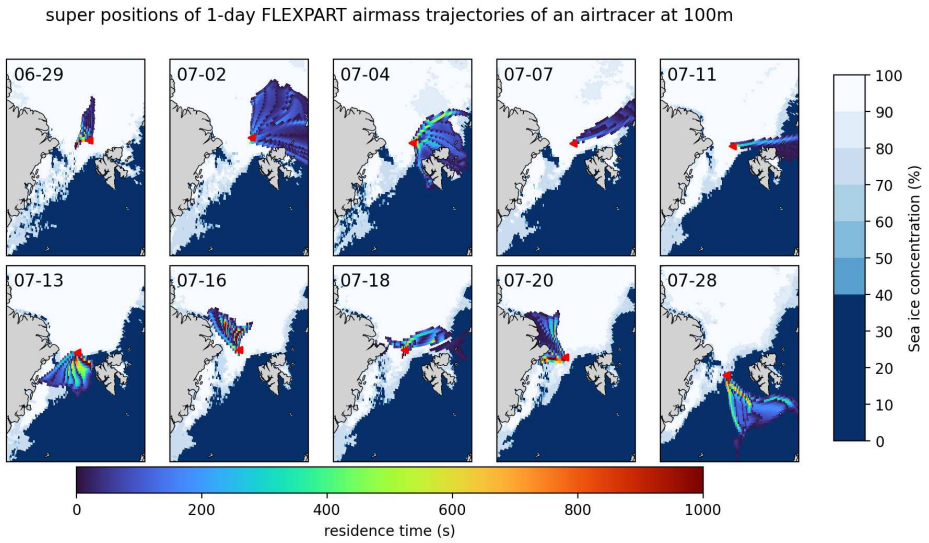

Figure A.3: Superimposed 1-day FLEXPART trajectories of a 100 m airtracer during each on-ice filter sample period (3-hr resolution) overlaid on the regridded MASAM2 daily-averaged sea ice concentrations.

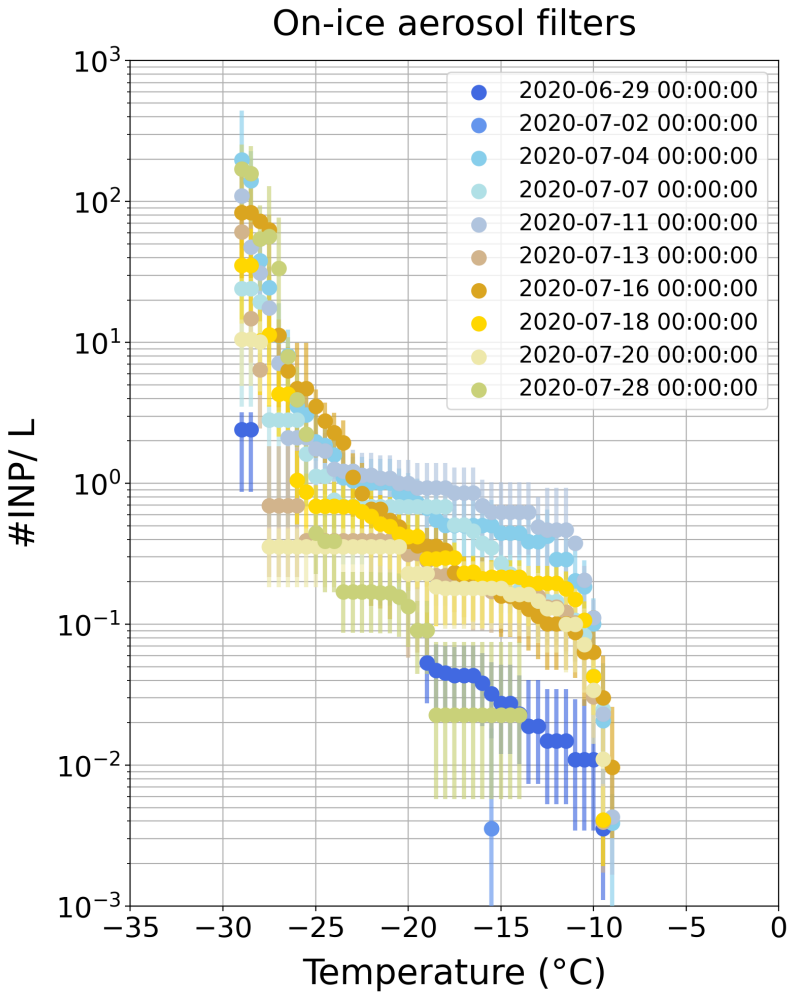

Figure A.4: Cumulative INP concentration as a function of temperature for samples collected on aerosol filters deployed on the ice, downwind of open water sources.

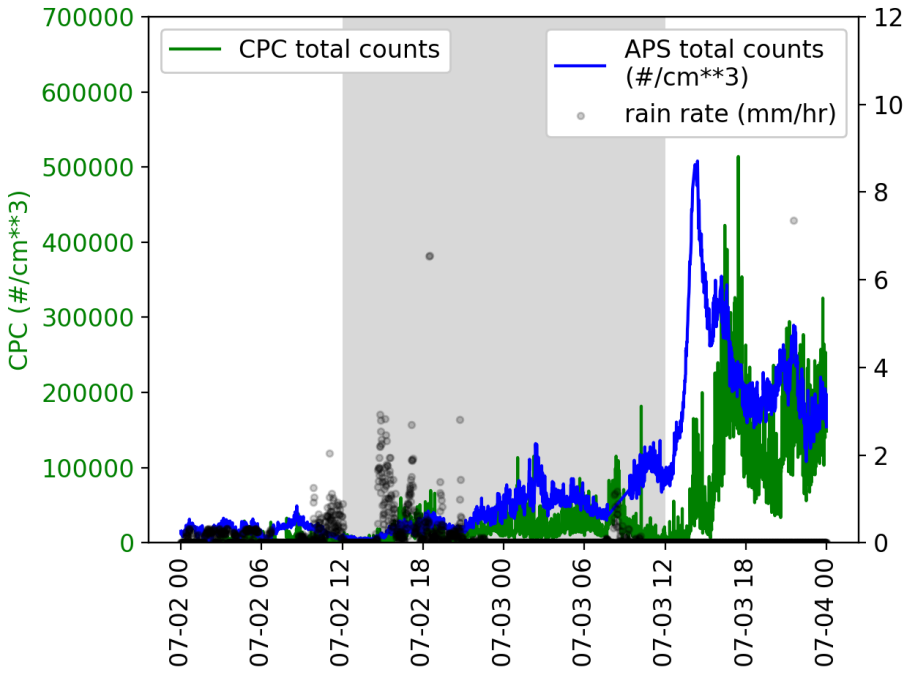

Figure A.5: Time series of minutely: rain rate (mm/hr) as measured by the present weather detector located at Met City (black, right-axis), APS total particle counts (#/cm^3) (blue, right-axis), CPC total particle counts (#/cm^3) (green, left-axis). Grey shading indicates on-ice aerosol filter sampling period.

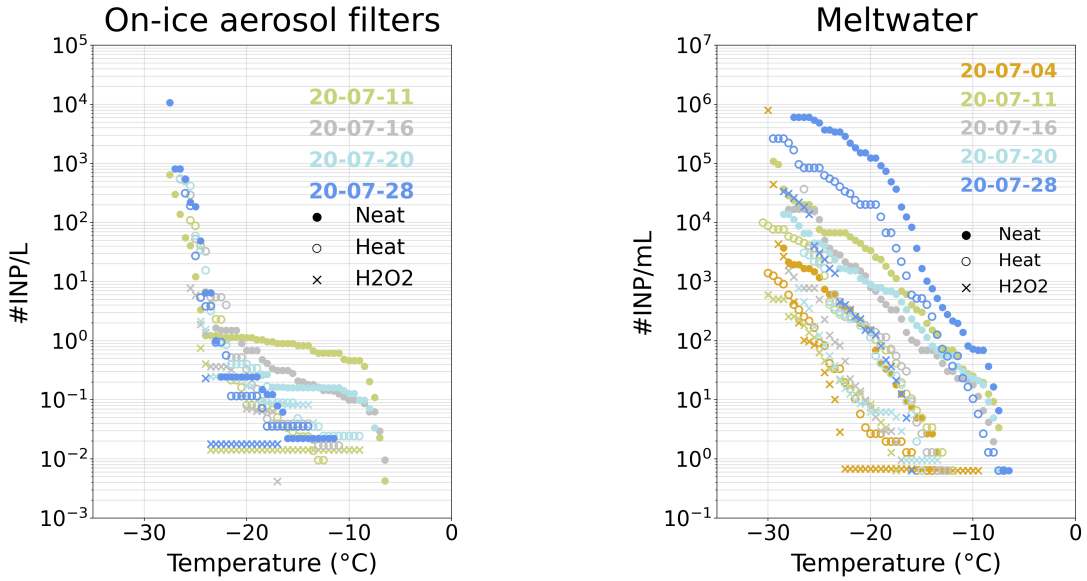

(a) **(b)**

Figure A.6: Cumulative INP concentration as a function of temperature for a subset of un-, heat, and peroxide treated (a) on-ice aerosol filter (b) meltwater

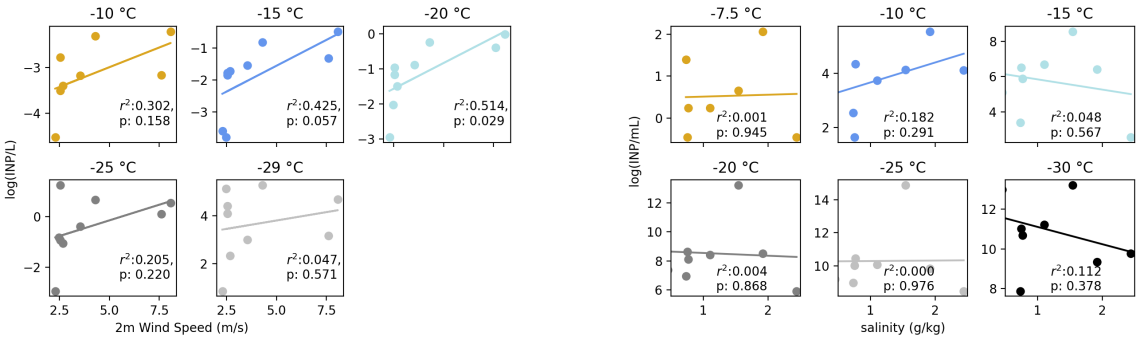

(a) **(b)**

Figure A.7: Scatter plots of (a) wind speed versus on-ice aerosol filter INP concentrations and (b) salinity versus meltwater INP concentrations at selected temperatures. Fitted regression line calculated using SciPy linear regression function. The r-squared and p- values are indicated within the figures

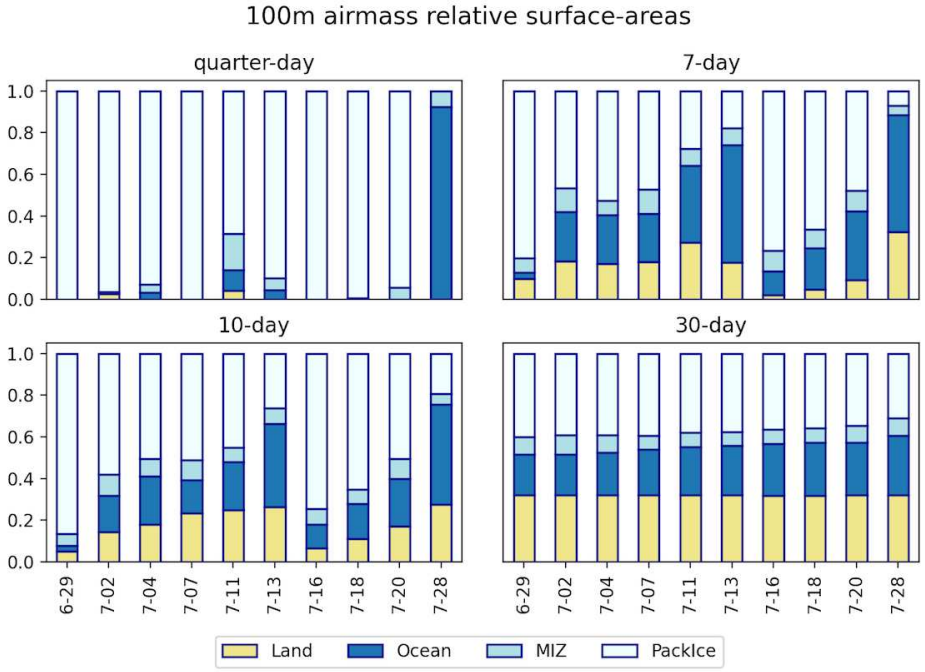

Figure A.8: Relative areal fraction of surface type passed over by FLEXPART simulated quarter, seven, ten and thirty-day 100 m air mass.

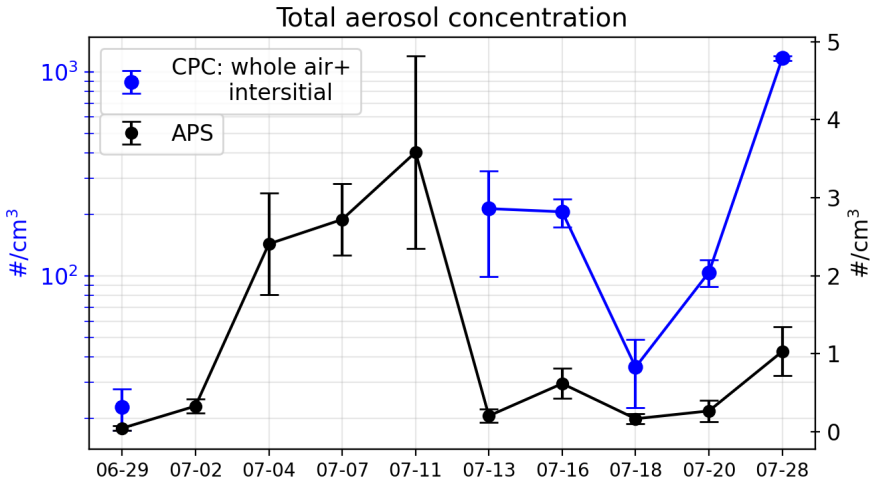

Figure A.9: Daily-averaged, corrected and pollution-filtered total particle counts (#/cm^3) measured by the APS (black, right-axis) and CPC (blue, left-axis) for each on-ice sampling day.

A.2 Supplemental Analyses

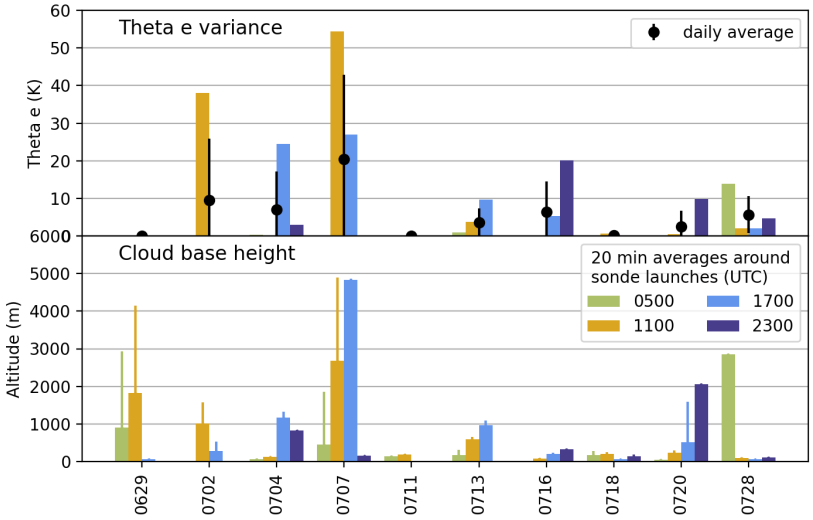

Figure A.10: (Top) Colored bars indicate 20-minute averaged potential temperature (theta e) variability centered around each radio-sonde launch (4-per day). Black circles (error bars) represent daily-averages (standard deviation) of potential temperature variability. (Bottom) Colored bars (error bars) indicate 20-minute averages (standard deviations) of first cloud base height centered around each radiosonde launch.

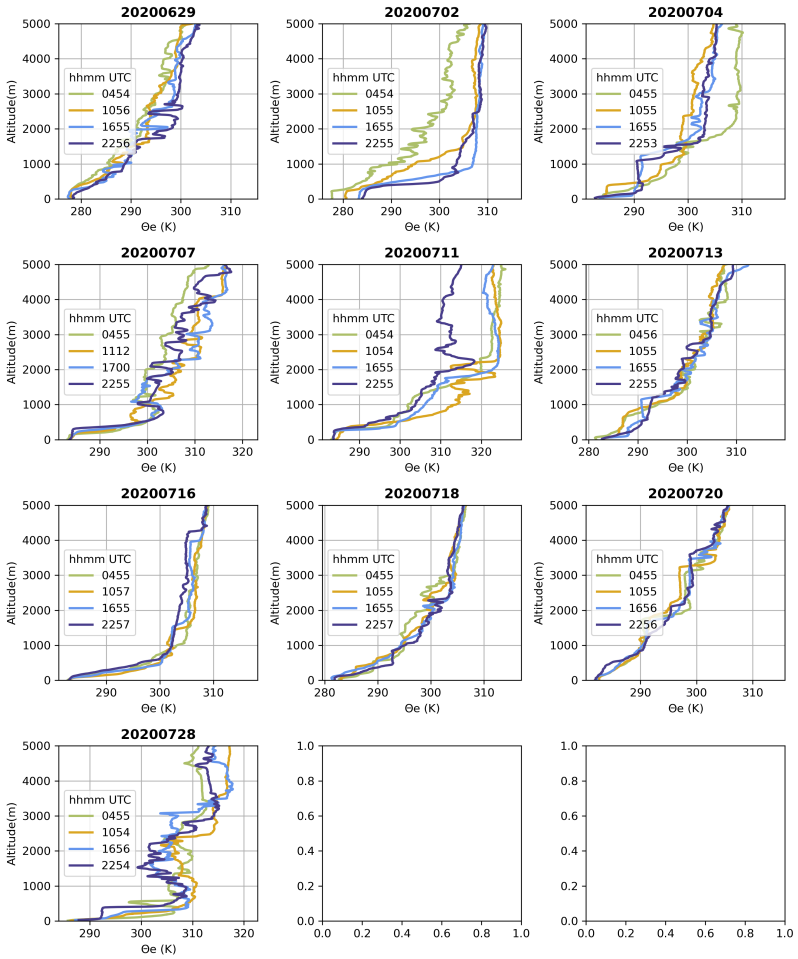

Figure A.11: Potential temperature (θ_e) profiles for each radiosonde launch for each sample day.

Cloud properties

Average cloud base heights 20 min surrounding each radiosonde launch (4 per day) were calculated from first-detected cloud base height values as measured by a ceilometer located on the P-Deck of *Polarstern* at 1-second resolution.[176] The data were filtered to include only periods when the detection status indicated the presence of at least one cloud base.

Atmospheric stability

For stability analysis, thermodynamic profiles from the surface to heights near 1 km were used. Those profiles are primarily based on Vaisala RS41-SGP radiosondes that were launched

every 3-6 hours from the helideck of *Polarstern* with a vertical resolution of 5 minutes. The lowermost 100 m of the sonde data were corrected for potential errors arising from the ship's impact on the measurement. Additionally, an extension of the lowermost 10 m was created using the meteorological tower within Met City. The data set and more details are available in Dahlke et al. (2023).[177] From these, profiles of equivalent potential temperature (θ_e) were then calculated using Eqs. (22) and (43) in Bolton et al. (1980).[178] Below-cloud θ_e variance was calculated employing NumPy's variance function (A.1) on the θ_e profiles from 10 m to the 20 min-average cloud base heights calculated as described above.

$$\mathrm{Var}(\theta_\mathrm{e}) = \mathrm{mean}(|x - \bar{x}|^2) \tag{A.1}$$

Boundary layer characteristics and cloud surface coupling

Many of the sampling days were characterized by a well-mixed environment beneath low clouds (**Figure A.9**). These observations aligned with those reported in Jozef et al. (2024)[112] that suggested the high moisture content during the MOSAiC summer eroded typically strong surface inversions.[111] A stratified below-cloud environment would suggest the surface is decoupled from higher altitudes and long-range influences. The days experiencing a stratified below-cloud environment include July 7, in which the potential temperature variance remained high throughout the day (**Figure A.10**). However it appears the wind speeds were a greater influence on the on-ice aerosol INPs than below-cloud environment variance for July 4 - 11. Another day with a distinctly stratified below-cloud environment is July 16, where there was an observed inter-sample spike for the cold INP population. June 29 and July 16 share similar atmospheric characteristics except for the below-cloud environment structure, which may have facilitated the distinct influence on the cold INP population on July 16. On July 28, the southerly air mass from the open ocean clearly influenced the strong below-cloud environment stratification on the MOSAiC ice station floe (**Figure A.10**). However, the on-ice aerosol INPs displayed a signature marine INP spectra, further

indicating stratification of the below-cloud environment may not have had a large influence on INPs detected near the surface.

A.3 Data Tables

Table A.1: Metadata for total aerosol filters sampled by the TRAPS package and meltwater samples on the ice. Locations are with respect to the Central Observatory on the MOSAiC floe (Figure S11). Geolocations of the floe are shown in Figure 1.

Location	**Start time (UTC YYYY-MM-DD hh:mm)**	**End time (UTC YYYY-MM-DD hh:mm)**	**Total volume (sL)**	**meltwater salinity (g/kg)**
Near melt pond A at Flux site	2020-06-29 11:42	2020-06-30 17:42	1077	No sample
Near melt pond B at Flux site	2020-07-02 13:27	2020-07-03 19:27	1074	0.73
Melt pond (James pond) near Balloon Town	2020-07-04 11:27	2020-07-05 14:51	984	2.44
Ponds near Balloon Town	2020-07-07 11:18	2020-07-08 14:10	475	0.09
Ponds near remote sensing	2020-07-11 10:58	2020-07-12 13:58	887	0.08
River near Met City	2020-07-13 11:07	2020-07-14 14:57	968	0.22
River near Met City	2020-07-16 11:26	2020-07-17 16:30	393	0.15
Lead near stern	2020-07-18 10:56	2020-07-19 13:02	932	No sample
Melt pond (James pond) near Balloon Town	2020-07-20 13:16	2020-07-21 16:04	346	0.15
Melt pond (James pond) near Balloon Town	2020-07-23 11:09	2020-07-24 11:18	0	0.38
Lead near stern	2020-07-28 11:34	2020-07-29 15:08	341	0.31

Table A.2: Metadata for total aerosol filters collected on the DOE-ARM AMF2 facility on the P-Deck of *RV Polarstern* during July 2020. GPS data from Ferrybox underway system.

Start		Stop		
Time (UTC YYYY-MM-DD hh:mm)	**Location - nearest hour (Lat, Lon)**	**Time (UTC YYYY-MM-DD hh:mm)**	**Location - nearest hour (Lat, Lon)**	**Total volume (sL)**
2020-07-03 16:05	(81.678958, 7.316884)	2020-07-06 15:05	(81.677137, 5.307839)	66197
2020-07-09 15:57	(81.530542, 2.557300)	2020-0712 17:30	(81.442827, 0.413012)	75741
2020-07-12 17:40	(81.442472, 0.410387)	2020-07-15 15:47	(81.292577, 0.316009)	101271
2020-07-15 15:56	(81.290093, 0.319182)	2020-07-18 15:35	(81.017158, 0.379824)	102636
2020-07-18 15:40	(81.007952, 0.352063)	2020-07-21 15:38	(80.591254, -0.621020)	88647

Table A.3: Metadata for snowpit samples.

Date UTC	**Location(Lat, Lon)**	**Depth (cm)**	**Characteristic**
2020-06-13	(82.130768, 7.702773)	41-39	Snow drift, new, wet
2020-06-27	(81.9695, 9.9059)	33-31	Wet, surface crust
2020-06-28	(81.8765, 9.4666)	40-39	New, wet
2020-07-07	(81.637918, 4.481572)	24-22	Wet
2020-07-24	(80.1873, -0.5909)	6-3	Ridge (14m)

Table A.4: Metadata for ice core, analogous FSW, and combined samples.

Ice Core (IC)				FSW		IC + FSW
Date (UTC YYYY-MM-DD)	**Location (Lat, Lon)**	**Depth(cm); t=top; b=bottom; m=middle 10cm**	**Sample volume factor**	**Date (UTC YYYY-MM-DD)**	**Salinity (g/kg)**	**Salinity (g/kg)**
2019-11-18	(85.849571, 120.581451)	t0-10, m	0.524, 0.528	2019-11-19	29.675	14.12, 14.00
2019-12-02	(85.930550, 113.592110)	t0-10, t20-30, m, b0-5	0.451, 0.531, 0.515, 0.531	2019-12-02	29	15.93, 13.59, 14.08, 13.59
2020-03-30	(85.365387, 13.091900)	t01-10, m, b0-5	0.498,0.50, 0.544	2020-03-30	29.55	14.83. 14.50, 13.48
2020-04-27	(83.917641, 15.562050)	m, b0-5	0.503, 0.536, 0.518	2020-04-26	31.125	15.48, 14.43, 15.00
2020-05-04	(83.886208, 18.240580)	t0-10, m, b0-5	0.513, 0.505, 0.518	2020-05-04	30.05	14.62, 14.86, 14.49
2020-07-20	(80.742088, -0.541270)	t0-10, m, b0-5	0.531, 0.479, 0.440	2020-07-20	28.225	13.23, 14.70, 15.8
2020-07-29	–	t0-10, b0-5	0.516, 0.464	2020-07-29	28.1	13.60, 15.05

Table A.5: Metadata for July 2020 BSW samples

Date (UTC YYYY-MM-DD hh:mm)	**Location (Lat, Lon)**	**Salinity (g/kg)**
2020-07-01 14:30	(81.762451, 8.85181)	33.50
2020-07-08 18:35	(81.5812, 2.91206)	33.00
2020-07-10 21:06	(81.479538, 2.08714)	–
2020-07-11 18:00	(81.450478, 1.20799)	34.0
2020-07-13 21:02	(81.406662, 0.25795)	33.00
2020-07-14 16:52	(81.36013, 0.28024)	–
2020-07-15 15:23	(81.29171, 0.31702)	–
2020-07-16 18:00	(81.207138, 0.28304)	–
2020-07-19 17:20	(80.860893, -0.31754)	–
2020-07-20 15:00	(80.741112, -0.54358)	32
2020-07-22 21:25	(80.421417, -0.48585)	–
2020-07-25 19:09	(79.887329, -1.15549)	–
2020-07-28 14:46	(79.322601, -2.70494)	–
2020-07-31 8:53	(79.071579, -2.82249)	–